RSC Advances

PAPER

View Article Online
View Journal | View Issue

Cite this: *RSC Adv.*, 2026, **16**, 10822

Synergistic beeswax-based nano-formulation for enhanced chronic wound healing and antibacterial potency

Ahmed M. Eid,[a] Abdullah S. Alawami,[b] Ahmed A. Allam,[b] Samar M. Mahgoub,[c] Ahmed G. Soliman,[d] Nashwa Shahin,[e] Roushdy M. M. *[a] and Rehab Mahmoud [f]

Chronic wounds, affecting over 10.5 million U.S. Medicare beneficiaries and exacerbated by diabetes, represent a critical healthcare challenge due to multifactorial pathophysiology, antimicrobial resistance, and inadequate therapeutic delivery. To address these limitations, we developed a novel beeswax-encapsulated emulsified formulation (F4) combining delafloxacin (DLX), lidocaine (LIDO), and sodium hyaluronate (SHA). F4 demonstrated high encapsulation efficiency (87.6–91.3%), optimal nanoparticle characteristics (115.68 nm, PDI 0.26, zeta potential −31.70 mV), and pH-responsive sustained release (94–100% cumulative release at 24 h, pH 7.4). Kinetic modeling confirmed a diffusion-controlled release mechanism (Korsmeyer–Peppas R^2 > 0.989), and comprehensive forced degradation studies coupled with *in silico* toxicological profiling (following ICH M7 guidelines) confirmed the formulation's stability and low impurity risk. Critically, F4 exhibited significantly enhanced antibacterial activity *versus* free DLX: larger inhibition zones against all tested pathogens (Gram-positive: *S. aureus*, *B. subtilis*; Gram-negative: *E. coli*, *P. aeruginosa*), 4-fold lower MICs against *S. aureus* (0.031 *vs.* 0.125 μg mL^{-1}) and *E. coli* (0.031 *vs.* 0.125 μg mL^{-1}), and potent bactericidal effects (MBC/MIC ≤ 2). F4 also disrupted biofilms at sub-MIC levels (1/16–1/64 MIC), comparable to ciprofloxacin, and achieved complete bactericidal killing of planktonic *S. aureus* within 12 h at 4× MIC. Furthermore, time-kill kinetics demonstrated a concentration-dependent bactericidal effect. Cytotoxicity assays confirmed enhanced biocompatibility (CC_{50}: 872.40 μg mL^{-1}), preserving >80% fibroblast viability at therapeutic doses. This multimodal platform concurrently addresses infection control (including biofilm resistance), analgesia, tissue regeneration, and controlled delivery, offering a transformative strategy for chronic wound management.

Received 29th August 2025
Accepted 20th January 2026

DOI: 10.1039/d5ra06488k

rsc.li/rsc-advances

1. Introduction

Chronic wounds, particularly those affecting diabetic and non-diabetic patients with compromised healing mechanisms, represent a significant healthcare burden worldwide. Chronic wounds affect 10.5 million (up 2.3 million from the 2014 update) of U.S. Medicare beneficiaries and impact the quality of life of nearly 2.5% of the total population of the United States.[1] The diabetic population continues to expand globally, with 14% of adults aged 18 years and older living with diabetes in 2022, an increase from 7% in 1990.[2] Diabetes was responsible for 3.4 million deaths in 2024; 1 every 9 seconds, and caused at least USD 1 trillion dollars in health expenditure.[3] These wounds often occur in patients with diabetes mellitus due to impairment of wound healing, leading to major causes of morbidity and mortality and representing the leading cause of major lower extremity amputation in the United States. The complexity of chronic wound pathophysiology involves multiple interconnected factors including persistent inflammation, bacterial colonization, impaired angiogenesis, and disrupted cellular proliferation and migration phases that collectively prevent normal wound closure.

Current therapeutic modalities for chronic wound management encompass a broad spectrum of interventions. Traditional approaches include wound debridement and dressing, transcutaneous electrical nerve stimulation (TENS), nanomedicine, shockwave therapy, and hyperbaric oxygen therapy (HBOT).[4] Despite these diverse treatment options, conventional therapies

[a]*Department of Botany and Microbiology, Faculty of Science (Boys), Al-Azhar University, Nasr City, Cairo 11884, Egypt. E-mail: mohamedali.125@azhar.edu.eg; aeidmicrobiology@azhar.edu.eg*

[b]*Department of Biology, College of Science, Imam Mohammad Ibn Saud Islamic University (IMSIU), Riyadh 11623, Saudi Arabia. E-mail: asalawam@imamu.edu.sa; aallam@imamu.edu.sa*

[c]*Materials Science and Nanotechnology Department, Faculty of Postgraduate Studies for Advanced Sciences, Beni-Suef University, Egypt. E-mail: miramar15@yahoo.com*

[d]*Biotechnology Program, Faculty of Agriculture, Ain Shams University, Cairo, Egypt. E-mail: Ahmedgamal_soliman@agr.asu.edu.eg*

[e]*Department of Chemistry, Faculty of Science (Girls), Al-Azhar University, Nasr City, Cairo 11884, Egypt*

[f]*Chemistry Department, Faculty of Science, Beni-Suef University, Beni-Suef 62511, Egypt. E-mail: rehabkhaled@science.bsu.edu.eg*

face several critical limitations that compromise their effectiveness in achieving optimal wound healing outcomes. Standard wound care protocols primarily focus on maintaining moisture balance, preventing secondary infections, and promoting granulation tissue formation through passive mechanisms. However, these approaches often fail to address the underlying molecular and cellular dysfunction characteristic of chronic wounds. The inability to simultaneously target multiple pathophysiological pathways results in suboptimal healing rates, prolonged treatment duration, and increased risk of complications including amputation. Furthermore, conventional antibiotic therapies face increasing challenges due to emerging antimicrobial resistance patterns. The extensive use of fluoroquinolones has been consequently accompanied by the emergence of bacterial resistance, which triggers the necessity to discover new compounds.[5] Traditional antibiotics often demonstrate reduced efficacy in the acidic, biofilm-rich environment characteristic of chronic wounds, necessitating the development of more sophisticated therapeutic approaches.

Delafloxacin represents a breakthrough in fluoroquinolone antibiotic development, offering unique advantages for wound healing applications. Delafloxacin is a novel anionic non-zwitterionic fluoroquinolone with enhanced antibacterial efficacy in acidic environments.[6] This characteristic is particularly relevant for chronic wound management, as wound beds typically maintain acidic pH conditions due to inflammatory processes and bacterial metabolism. Clinical evidence demonstrates delafloxacin's superior efficacy in treating skin and soft tissue infections. In clinical trials involving cellulitis/erysipelas, major cutaneous abscess, and wound infections, delafloxacin achieved a cure rate of 70.4%, compared to linezolid's cure rate of 64.9% and vancomycin's cure rate of 54.1% ($P = 0.031$).[7,8] The broad-spectrum antimicrobial activity of delafloxacin against both Gram-positive and Gram-negative organisms, including resistant strains such as MRSA, makes it particularly suitable for the polymicrobial environment often encountered in chronic wounds.[9]

Pain management represents a critical component of chronic wound care, as persistent pain significantly impacts patient quality of life and may interfere with healing processes. Lidocaine, a well-established local anesthetic, provides immediate pain relief through sodium channel blockade, enabling comfortable wound care procedures and improving patient compliance with treatment protocols.[10,11] Beyond its analgesic properties, lidocaine demonstrates additional therapeutic benefits relevant to wound healing. The agent exhibits anti-inflammatory effects that may help modulate the excessive inflammatory response characteristic of chronic wounds. Furthermore, lidocaine's membrane-stabilizing properties can protect cellular structures from oxidative damage and promote cellular viability in the wound environment.[12]

Sodium hyaluronate serves as a cornerstone component in advanced wound healing formulations due to its multifaceted biological activities. Hyaluronan is a versatile, polymorphic glycosaminoglycan with vast biological functions, found throughout the body and primarily residing in skin, thus playing an important role in wound healing.[13] Its hydrophilic nature enables superior moisture retention, creating an optimal microenvironment for cellular proliferation and migration.[14] The wound healing properties of sodium hyaluronate extend beyond simple hydration. Sodium hyaluronate avoids tissue dehydration and supports the healing process through its porous structure. Additionally, hyaluronic acid facilitates angiogenesis, stimulates fibroblast proliferation, and modulates inflammatory responses, collectively accelerating the transition through wound healing phases. Recent research has demonstrated synergistic effects when hyaluronic acid is combined with other therapeutic agents. HA conjugates interact with skin cells through multiple receptor types, resulting in synergistically improved healing effects. This finding supports the rationale for incorporating sodium hyaluronate into multi-component wound healing formulations.[15]

Beeswax serves as both an encapsulation matrix and an active therapeutic component in wound healing applications.[16] As a natural biocompatible material, beeswax provides controlled release properties that ensure sustained delivery of active pharmaceutical ingredients to the wound bed. The occlusive properties of beeswax create a protective barrier that maintains wound hydration while preventing external contamination. Clinical evidence supports the wound healing benefits of beeswax-containing formulations. Beeswax-olive oil-butter mixture impregnated bandage treatment improved burn wound healing and encouraged skin renewal *via* modulating tissue TGF-β1 and VEGF-α.[17] The natural antimicrobial properties of beeswax complement the antimicrobial action of delafloxacin, providing additional protection against wound colonization.[18]

The combination of delafloxacin, lidocaine, and sodium hyaluronate within a beeswax encapsulation system represents a rational approach to addressing the multifactorial nature of chronic wound pathophysiology. This formulation strategy targets multiple therapeutic objectives simultaneously: antimicrobial action against resistant pathogens, pain management for improved patient comfort, enhanced tissue regeneration through hyaluronic acid activity, and controlled drug delivery *via* beeswax encapsulation. The synergistic potential of these components lies in their complementary mechanisms of action. While delafloxacin addresses the infectious component of chronic wounds, sodium hyaluronate promotes cellular regeneration and angiogenesis. Lidocaine facilitates pain-free wound care and may contribute anti-inflammatory effects, while beeswax ensures sustained release and provides additional antimicrobial protection. The combination of multiple active agents offers synergistic effects that promote faster wound healing while preventing infections, which is crucial in wound management where infection risk is high.

The primary aim of this study is to develop and characterize a novel encapsulated emulsified formulation containing delafloxacin, lidocaine, and sodium hyaluronate in a beeswax matrix for the treatment of chronic and difficult-to-heal wounds in both diabetic and non-diabetic patients. This research addresses the critical need for advanced wound care solutions that can simultaneously target multiple pathophysiological pathways while providing sustained therapeutic delivery. The novelty of this approach lies in several key aspects: first, the utilization of delafloxacin, a next-generation fluoroquinolone

with enhanced activity in acidic wound environments; second, the synergistic combination of antimicrobial, analgesic, and regenerative components within a single formulation; third, the employment of beeswax as a natural, biocompatible encapsulation system that provides controlled release while contributing therapeutic benefits; fourth, a comprehensive assessment of the formulation's stability, impurity profile, and *in silico* toxicological risk in accordance with ICH guidelines, ensuring a high safety standard; and fifth, the development of an emulsified delivery system that enhances bioavailability, wound penetration, and demonstrates superior antibiofilm and bactericidal kill kinetics compared to the free antibiotic. This innovative formulation represents a paradigm shift from conventional single-target therapies toward a comprehensive, multi-modal wound healing approach. By concurrently addressing infection control (including resilient biofilms), pain management, tissue regeneration, cytocompatibility, and sustained drug delivery within a single therapeutic system, this research aims to establish new standards for chronic wound care and potentially reduce the burden of non-healing wounds in vulnerable patient populations.

2. Experimental section

2.1. Materials

Beeswax (BW) with a melting point of 60–66 °C and purity of 99%, sodium acetate trihydrate, monobasic potassium phosphate, diammonium hydrogen phosphate, and soya been lecithin were purchased from Sigma Chemical Co (St Louis, Missouri, United States). Delafloxacin (DLX) with purity 99.82% was obtained from METROCHEM API PRIVATE LIMITED company, India. Sodium hyaluronate (SHA) with purity 99.49% was purchased from MANUS AKTTEVA BIOPHARMA LLP, Gujarat, India. Lidocaine hydrochloride (LIDO) with purity 99.92%, Tween-80, acetonitrile, hydrochloric acid 37%, and ethanol were purchased from Merck, Darmstadt, Germany. Dimethyl sulfoxide (DMSO), MTT, and trypan blue dye were purchased from Sigma (St. Louis, Mo., USA). Additionally, fetal bovine serum, DMEM, HEPES buffer solution, L-glutamine, and gentamycin were purchased from Lonza (Belgium), distilled water.

2.2. Formulation development and encapsulation of in beeswax

The encapsulation process was conducted upon four formulations depending on the percentage of beeswax, Tween 80 as shown in Table 1. Each formulation involved encapsulating of SHA, LIDO and DLX in beeswax using a nano-emulsion method.[19,20] The process begins with preparing an oily phase by melting beeswax at 90 °C in a water bath. Then, soya lecithin is added and stirred, followed by the incorporation of SHA, LIDO and DLX after their dissolving in 20 mL 50% ethanol into the mixture. Simultaneously, an aqueous phase is prepared by dissolving of Tween 80 in 30 mL of purified water at 70 °C. The aqueous phase is then added to the molten oily phase with continuous stirring for 2 hours with a magnetic stirrer, resulting in the formation of an emulsion. This emulsion is subsequently sonicated using an ultrasonic bath, followed by stirring with a magnetic stirrer until it cools to room temperature, ensuring proper encapsulation and stability of the bioactive compounds.

2.3. Selection of the best formulation

2.3.1. Determination of encapsulation of SHA, LIDO and DLX in beeswax (EE%). The encapsulation efficiency was determined chromatographically using an HPLC 1260 Infinity II instrument provided by a quaternary pump, a DAD detector, and an autosampler (Agilent, USA). The separation was carried out using an Inertsil ODS-3-C18 column (250 × 4.6 mm, 3 μm particle size; Agilent Technologies, USA). The injection volume was 25 μL, and an isocratic elution program was applied using a mobile phase consisting of 0.0101 M phosphate buffer (dissolving 1.32 g of diammonium hydrogen phosphate in 1 L distilled water and adjust pH to 7) and acetonitrile in ratio 1 : 1, at a flow rate of 1 mL min^{-1}. Detection was performed at dual wavelength of 205 nm and 265 nm for SHA, DLX and LIDO, respectively under ambient temperature. Calibration curves were prepared by varying concentrations of SHA, LIDO and DLX, each one separately in 50% ethanol as diluent, followed by mobile phase for final dilutions, Fig. 1A.

For each formula, transfer 25 mL of formed emulsion to 50 mL of 50% ethanol followed by mobile phase to get final dilutions and subjected to centrifugation at 10 000 rpm for 15 minutes. The supernatant was then analyzed using the HPLC system at the dual wavelengths to quantify the amount of sodium hyaluronate (SHA), Lidocaine HCl (LIDO) and delafloxacin (DLX) loaded in the beeswax,[21] as shown in Fig. 1B. The encapsulation efficiency was calculated by subtracting the free active components in the supernatant from the total amount of each component initially added during formula preparation, eqn (1)–(3):

Table 1 Formulations containing equal amounts of SHA, LIDO and DLX, with variations in beeswax and Tween 80 to determine the optimal formulation

Ingredients	Formulation 1 (F1)	Formulation 2 (F2)	Formulation 3 (F3)	Formulation 4 (F4)
SHA (mg)	100	100	100	100
LIDO (mg)	100	100	100	100
DLX (mg)	100	100	100	100
Beeswax (mg)	300	500	400	500
Soya lecithin (mg)	150	150	150	150
Tween 80 (mg)	150	150	300	300
Purified distilled water (mL)	50	50	50	50

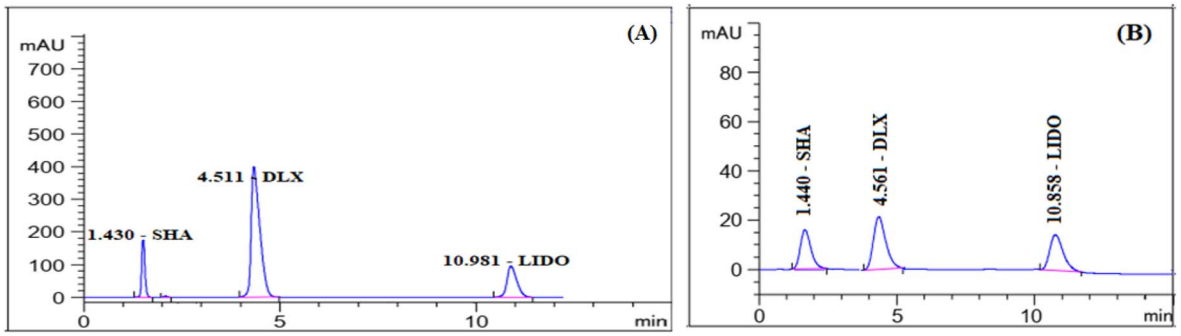

Fig. 1 (A) HPLC chromatograms of SHA, DLX and LIDO recorded at the dual wavelengths of 205 nm and 265 nm. The concentration of each drug solution is 100 μg mL^{-1}, (B) HPLC chromatograms of encapsulated SHA, DLX and LIDO in beeswax recorded at the dual wavelengths of 205 nm and 265 nm.

$$\text{Encapsulation efficiency for SHA } \% = \frac{\text{total amount of SHA} - \text{free SHA}}{\text{total amount of SHA}} \quad (1)$$

$$\text{Encapsulation efficiency of LIDO} = \frac{(\text{total amount of LIDO} - \text{free LIDO})}{\text{total amount of LIDO}} \quad (2)$$

$$\text{Encapsulation efficiency of DLX} = \frac{(\text{total amount of DLX} - \text{free DLX})}{\text{total amount of DLX}} \quad (3)$$

2.3.2. Particle size distribution, PDI, and zeta potential for loaded and un loaded beeswax. The Zetasizer Ultra (Malvern, USA) was used to determine the size, dimension, polydispersity index (PDI), and zeta potential of the loaded and unloaded beeswax. The zeta potential and Dynamic Light Scattering (DLS) techniques provide insight into the particle size distribution, surface charge, PDI, and stability of the encapsulated formulation.[22]

2.4. Characterization of the encapsulated particles

The selected encapsulated formulation has been characterized using different techniques to confirm the physicochemical properties of the bioactive compounds and the encapsulation efficiency such as Bruker-Vertex 70 Spectrometer (Germany) apparatus covering the wave number range of 4000–400 cm^{-1} was used for Fourier Transform Infrared Spectroscopy (FTIR) investigation, and transmission Electron Microscopy (TEM) to assess the crystallinity, chemical composition, and morphology of the particles.

2.5. *In vitro* release study

The *in vitro* release study evaluated the dissolution profiles of delafloxacin (DLX), lidocaine hydrochloride (LIDO), and sodium hyaluronate (SHA) from a beeswax-encapsulated formulation (F4) across four physiologically relevant media: HCl pH 1.2 (8.5 mL of concentrated hydrochloric acid 37% to approximately 900 mL of distilled water, mix well, and adjust the pH to 1.2 using either diluted HCl or 1 N NaOH as needed. Make up the final volume to 1 L with distilled water), acetate buffer pH 4.5 (by Dissolving 3.5 g of sodium acetate trihydrate in 900 mL of distilled water, then add 1.2 mL of glacial acetic acid. Adjust the pH to 4.5 using acetic acid or 1 N NaOH if needed, and bring the total volume to 1 L with distilled water. Mix thoroughly), phosphate buffer pH 6.8 (by dissolving 6.8 g of monobasic potassium phosphate (KH_2PO_4) in 900 mL of distilled water and adjusting the pH to 6.8 using 0.2 N NaOH. Make up the volume to 1 L with distilled water), and PBS with 0.5% SLS pH 7.4 (by dissolving 8.0 g NaCl, 0.2 g KCl, 1.44 g Na_2HPO_4, 0.24 g KH_2PO_4, and 5.0 g sodium lauryl sulfate (SLS) in 900 mL of distilled water. Adjust the pH to 7.4 using 1 N NaOH or 1 N HCl, and complete the volume to 1 L). Using a USP Dissolution Tester (Apparatus 2, 50 rpm, 37 °C), 5 mL of F4 was added to 500 mL of each medium along 6 separate vessels, with samples withdrawn at 0.25, 0.5, 1, 2, 4, 8, 12, 20, and 24 hours. Samples were filtered (0.45 μm), replaced with fresh medium, and analyzed *via* HPLC apparatus. Cumulative release percentages were calculated using corrected volume replacement, comparing F4 against an unencapsulated control solution.

Drug release at time t, cumulative drug release (%) were calculated using eqn (4) and (5):

$$\text{Released drug at time } t = C_t \times V \quad (4)$$

where, C_t represents the drug concentration at time t (mg mL^{-1}), V represents volume of the dissolution medium (mL).

$$\text{Cumulative drug release } (\%) = \frac{\text{released drug at time } t}{\text{initial amount of drug loaded}} \times 100 \quad (5)$$

2.6. *In vitro* release kinetics

Various release kinetics models were applied including zero-order kinetics (constant release rate), first-order kinetics (release rate depends on the amount of drug remaining), Korsmeyer–Peppas model (power law), Higuchi model (diffusion-controlled release) to give insight into the release mechanism either through diffusion, swelling, or erosion of the encapsulated formulation using the following equations:

Zero-order kinetics

$$M_t = M_\infty + K_t \quad (6)$$

First-order kinetics

$$\frac{M_t}{M_\infty} = 1 - e^{-k_1 t} \quad (7)$$

Korsmeyer–Peppas model

$$\frac{M_t}{M_\infty} = Kt^n \quad (8)$$

Higuchi model

$$M_t = k_H \sqrt{t} \quad (9)$$

M_t = amount of drug released at time t, M_∞ = initial amount of drug, k_1 = first-order rate constant, n is the release exponent that indicates the release mechanism, t = time, k_H = Higuchi rate constant (depends on properties like the diffusion coefficient, solubility, and surface area).

2.7. *In vitro* cytotoxicity and cell viability

2.7.1. Cell lines and culture conditions. Fibroblasts are critical to wound repair, orchestrating key processes such as collagen deposition, extracellular matrix (ECM) remodeling, and tissue regeneration. These functions are essential across all types of chronic wounds whether occurring in diabetic or non-diabetic individuals. Given that the developed formulation is designed to address infection, pain, and impaired healing in a broad spectrum of chronic wounds including diabetic foot ulcers (DFUs), venous leg ulcers (VLUs), and pressure ulcers. Human dermal fibroblasts (HDFs) were selected as a biologically relevant *in vitro* model. As they provide an ideal system to assess the regenerative and cytoprotective potential of the beeswax-encapsulated dual-drug delivery system across diverse chronic wound etiologies. The cells were obtained from the American Type Culture Collection (ATCC, Manassas, VA, USA) and cultured in Dulbecco's Modified Eagle's Medium (DMEM) supplemented with 10% heat-inactivated fetal bovine serum (FBS), 1% L-glutamine, HEPES buffer, and 50 μg mL^{-1} gentamicin. Cultures were maintained at 37 °C in a humidified 5% CO_2 incubator and subcultured biweekly to preserve healthy, proliferative cell populations.

2.7.2. Cytotoxicity evaluation *via* MTT assay. The cytotoxic effects of the formulated delivery system were assessed using the MTT assay, a well-established method for evaluating cellular metabolic activity as an indicator of viability. Human dermal fibroblasts (HDFs) were seeded into 96-well tissue culture plates at a density of 1×10^4 cells per well and allowed to adhere for 24 hours under standard culture conditions. After initial incubation, cells were exposed to increasing concentrations of the test formulations for an additional 24 hour period. All treatments were performed in triplicate, and each plate included untreated control wells to establish baseline viability (normalized to 100%) per ISO 10993-5 guidelines for medical device biocompatibility testing.[23–25]

The assay was validated using untreated HDFs as the negative control, consistent with ISO 10993-5 recommendations, which emphasize baseline viability assessment over positive controls for extractable cytotoxicity evaluation.[23,26]

Following treatment, the culture medium was carefully removed and replaced with 100 μL of fresh DMEM. Subsequently, 10 μL of MTT reagent (12 mM, prepared by dissolving 5 mg MTT in 1 mL phosphate-buffered saline) was added to each well. Plates were then incubated at 37 °C for 4 hours, during which viable cells reduced MTT to insoluble formazan crystals. After incubation, 85 μL of the medium was discarded, and 50 μL of dimethyl sulfoxide (DMSO) was added to dissolve the formazan. The plates were shaken gently to ensure complete solubilization, and absorbance was measured at 590 nm using a microplate reader.

Cell viability was calculated as a percentage of the optical density (OD) of treated cells relative to the OD of untreated control cells using the following equation:

$$\text{Percentage of viability} = [(OD_t/OD_c)] \times 100\% \quad (10)$$

where OD_t is the mean optical density of treated wells and OD_c is the mean optical density of untreated wells. Survival curves were constructed by plotting the percentage of viable cells against the tested material's concentration. The cytotoxic concentration (CC_{50}), which is the concentration required to induce toxic effects in 50% of the intact cells, was determined from the dose–response curve using GraphPad Prism software (San Diego, CA, USA).

2.8. Forced degradation studies and impurity risk assessment

2.8.1. Study design and conditions. A comprehensive forced degradation study was performed on the individual Active Pharmaceutical Ingredients (APIs) including sodium hyaluronate (SHA), lidocaine HCl (LIDO), and delafloxacin (DLX) as well as on the optimized beeswax-encapsulated formulation F4. The study followed ICH Q1A(R2) and Q1B guidelines to identify potential impurities, characterize degradation pathways, and confirm the stability-indicating capability of the analytical method. A targeted degradation range of 5–20% was established to ensure the formation of meaningful degradation products without inducing excessive breakdown of the parent compounds. In parallel, a targeted nitrosamine risk assessment was performed in alignment with FDA and EMA expectations, focusing on the structural alert associated with the secondary amine in lidocaine and the tertiary amines in delafloxacin.

The APIs and formulation were subjected to stress conditions selected to induce controlled degradation, including acidic and alkaline hydrolysis using 0.1 N HCl and 0.1 N NaOH at 25 °C for 6 hours; oxidative stress using 3.0% w/v hydrogen peroxide at 25 °C for 6 hours; thermal degradation by incubating solid samples at 60 °C for 5 days; and photolytic exposure to visible light for 2 days, in accordance with ICH Q1B. To evaluate nitrosamine formation potential, a worst-case nitrosating condition was applied using 0.01% w/v sodium nitrite in pH 3.0 acetate buffer at 37 °C for 18 hours.

At predetermined intervals, samples were collected, neutralized when necessary, diluted with the mobile phase, filtered through a 0.45 μm membrane, and immediately

analyzed using HPLC-DAD to quantify degradation and assess impurity profiles.

The analysis was performed using the HPLC system described in Section 2.3.1. The method employed DAD detection across 190–400 nm. To maximize the detection of potential impurities, including those with weak chromophores, chromatograms were analyzed at multiple wavelengths (205 nm, 230 nm, 265 nm, 280 nm). Peak purity was assessed for the main APIs to ensure no co-elution with degradation products.

2.8.2. *In silico* toxicity and genotoxicity assessment. A comprehensive *in silico* toxicological risk assessment was performed for the individual Active Pharmaceutical Ingredients (APIs) and the complete formulation in accordance with ICH M7 guidelines to evaluate impurity and genotoxicity risks. The assessment employed a multi-tiered computational approach.[27–29]

Forward reaction prediction was conducted using the ASKCOS webserver to evaluate the potential for chemical interactions between formulation components that could lead to novel impurity formation.[27]

Toxicity and genotoxicity profiling were performed using the Toxtree software (v3.1.0) with several modules.[28–31] Compounds were evaluated using the Cramer rules for systemic toxicity classification.[28] Structural alerts for genotoxicity were assessed using built-in rules for DNA binding (*via* electrophilic reaction chemistry)[29] and protein binding (covalent interaction potential).[30] Furthermore, the Toxtree modules for Ames test mutagenicity (based on structural alerts)[31] and carcinogenicity (non-genotoxic carcinogen alerts)[32] were applied. Molecular docking studies were conducted to quantify the binding affinity of the compounds to DNA, providing a quantitative measure of intercalation potential. The crystal structure of a DNA duplex (PDB ID: 1TUP) was used as the receptor. Ligand structures were energy-minimized, and molecular docking was performed using QVINA2 (ref. 33) following the AutoDock protocol for preparation. The binding affinity (ΔG, kcal mol^{-1}) for each compound was calculated and compared to ethidium bromide, a known DNA intercalator.

Organ-specific toxicity and acute toxicity classification were predicted using the ProTox3.0 webserver, which provides estimates for oral LD_{50} and probabilities for various organ toxicities (*e.g.*, hepatotoxicity, neurotoxicity).[34,35]

2.9. Microbiological analyses

2.9.1. Strains and culture conditions. All bacterial strains were friendly dedicated from Botany and Microbiology Department, Faculty of Science (Boys), Al-Azhar University (Cairo, Egypt). The strains that have been involved in the present study were *Bacillus subtilis* ATCC 6051, *Staphylococcus aureus* ATCC 29213 (as Gram positive strains), *Pseudomonas aeruginosa* ATCC 27853 and *Escherichia coli* ATCC 35218 (as Gram negative ones). The strains were preserved in glycerol under freezing at −80 °C and refreshed before using by culturing them in Tryptic Soya Agar (TSA) media (HiMedia, India).

2.9.2. Preparation of bacterial strains suspension. All bacterial strains in this study were prepared according to Clinical Laboratory Standards Institute (CLSI) guidelines.[36] The strains were sub-cultured on Muller Hinton Agar (MHA) media and left overnight under septic conditions at 37 °C. At the end of the incubation period, 3 growing bacterial colonies were selected and transferred to a 0.9% sterile saline solution and mixed vigorously using vortex mixer. The turbidity of the bacterial suspension was adjusted to 0.5 McFarland standard by carefully adding the bacterial suspension to McFarland solution [1% solution of anhydrous barium chloride (0.5 mL) and 1% solution of sulfuric acid (99.5 mL)]. A white background with contrasting black lines was used to achieve 0.5 McFarland standard where the colony count measures approximately 1.5×10^8 CFU mL^{-1}.

2.9.3. Resazurin stock solution preparation. The preparation of resazurin dye solution was carried out using the method of Teh *et al.*[37] by adding 337.5 mg of resazurin powder to 50 mL of sterile distilled water in a sterile flask and the resulted solution was vigorously mixed for 1 hour using sterile vortex mixer until achieving complete homogenization. The procedure was performed in a dark room and the prepared resazurin stock solution was kept in a dark brown bottle and prevented from exposure to light (where the solution is light sensitive).

2.9.4. Antibacterial activity assay. The potency of F4 encapsulated compound was tested for its antimicrobial using Agar well diffusion assay.[38] MHA (Oxoid) media was applied for the growth of the tested bacterial strains. The media was sterilized, poured in sterile Petri plates and left to cool at 45–50 °C and 1 mL of 0.5 McFarland standards (1.5×10^8 CFU mL^{-1}) of each bacterial strain was added inoculated into the media, mixed to get homogeneity and left to cool at room temperature. By using a sterile cork borer, a 6 mm well was bored and 100 μL of F4 encapsulated compound was introduced into the well. DLX as well as other ingredients (SHA, Lido, Beeswax, Soya lecithin and Tween 80) were loaded into the other wells (100 μL) for comparison of their antibacterial activity (if any). All plates were incubated at 37 °C for 24 h. At the end of incubation, the bacterial growth inhibition zones were determined, and the results were recorded using the guidelines of CLSI.[39] The interpretation of the resulting zones was as follows: less than 15 mm the examined compound will be considered as poorly active, while from 15–25 mm it will be considered as active, consequently more than 25 mm it will be highly active.[38]

2.9.5. Determination of minimum inhibitory concentration (MIC). Broth microdilution method was used for determination of minimum inhibitory concentration (MIC). The MIC was defined as the lowest concentration in which no growth can be detected. A sterile polystyrene 96-well plate with flat bottom (SPL, Korea) was used for determination of MIC of the tested F4 encapsulated compound (Scheme 1). To all the wells in the microtiter plate, 100 μL of MHB media was added from column 1 to column 12. The bacterial suspension (50 μL) of 0.5 McFarland standard (1.5×10^8 CFU mL^{-1}) was introduced into each well (3 rows for each strain). Lastly, Two-fold serial dilution of DLX or F4 encapsulated compound (at concentration of 512 μg mL^{-1}) fraction was prepared as 128, 32, 8, 2, 0.5, 0.125, 0.031, and 0.0078 μg mL^{-1} to evaluate minimum inhibitory concentration (MIC). 50 μL of each concentration was added to each

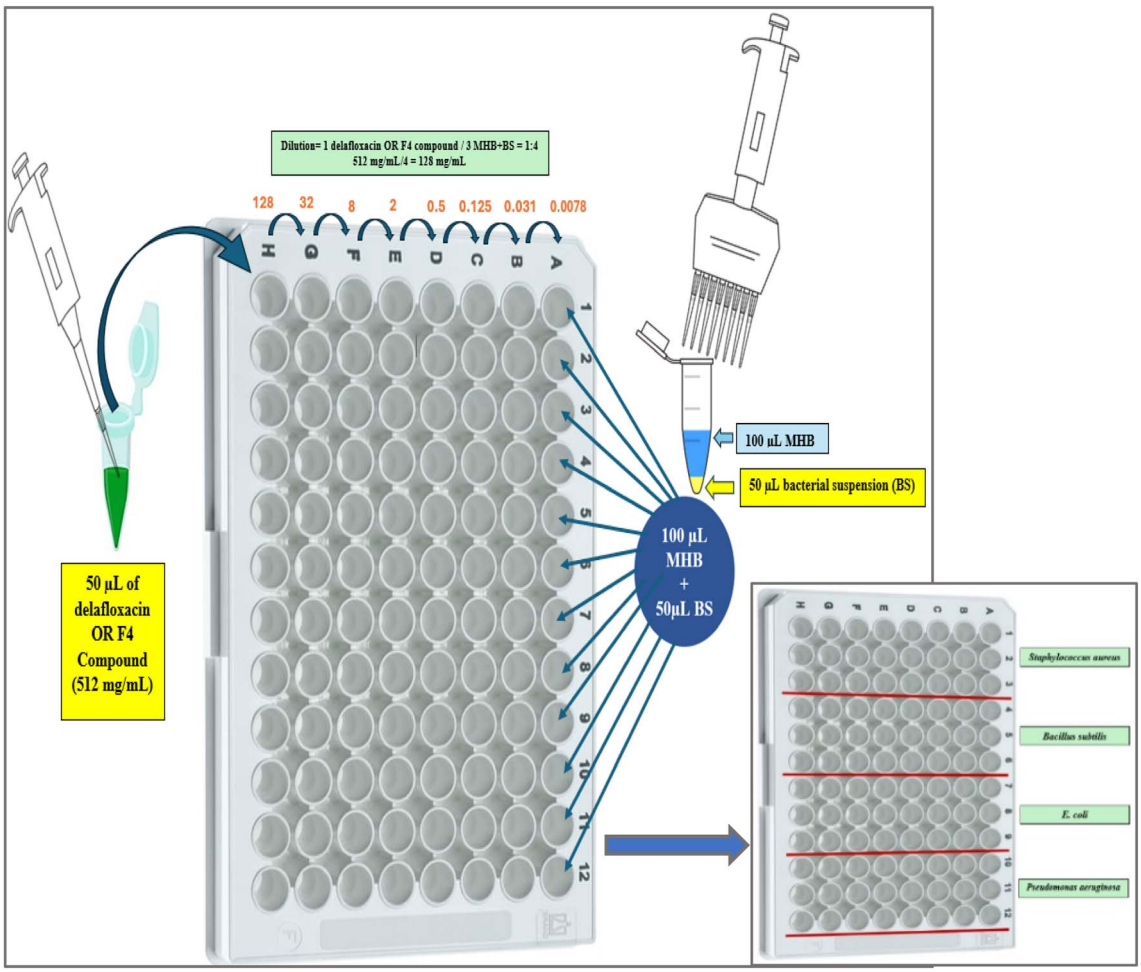

Scheme 1 A polystyrene 96-well plate with flat bottom was used for determination of MIC of the testing F4 encapsulated compound.

well where, the first concentration (128 μg mL^{-1}) in H-well was then serially diluted by transferring 50 μL of each well to the next well until receiving a concentration of 0.0078 μg mL^{-1} at the last well (A) from which 50 μL was discarded. The plates were incubated for 18 hours at 37 °C, then 20 μL resazurin solution (0.01%) was added and the plates were re-incubated for 2–4 hours after incubation the readings were performed at 630 nm using microtiter plate reader. The indicator dye (resazurin) serves as redox indicator which was oxidized in the acidic medium caused by bacterial metabolic activities enhancing the color change from blue (no detection of bacterial growth) to pink (resazurin is reduced to resorufin, which has a pink color).[39] Bacterial cultures without addition of DLX or F4 encapsulated compound were used as negative control. MIC was determined using CLSI guidelines[40] and three replicates of each assay were achieved, and the average of three independent experiments were recorded.

2.9.6. Minimum bactericidal concentration (MBC) assay. The MBC of F4 encapsulated compound was determined according to CLSI guidelines. To calculate the MBC, 10 μL from the wells that corresponded to the MIC value of the tested pathogens where no bacterial growth was visible, spread on the surface of MHA plate, incubated for 24 h at 37 °C, and the appearance or absence of bacterial colonies was observed. Three replicates of each experiment were performed. MBC was defined as the least concentration of the tested compound that reduce the bacterial viable count to 99.9% on MHA media. The experiment was carried out in triplicates.[41]

2.9.7. Biofilm inhibition assay. To determine biofilm inhibition, microtiter plate method was used. Firstly, each bacterial strain was seeded in trypticase soy broth (TSB) medium containing 1% (w/v) glucose and adjusted to 0.5 McFarland (1.5×10^8 CFU mL^{-1}). A sterile polystyrene 96-well plate with flat bottom (SPL, Korea) was used. To each well, 200 μL of TSB containing 1% (w/v) glucose was loaded into a 96-wells plate. Concentrations sub-MIC of F4 encapsulated compound was then loaded into the 96-wells plate and the bacterial strain suspension was serially diluted (2, 1, $\frac{1}{2}$, $\frac{1}{4}$, 1/8, 1/16, 1/32 and 1/64-MIC). The microplates were incubated for 24 hours at 37 °C. Following the incubation time, the microtiter wells were rinsed with 300 μL of phosphate buffer saline (pH = 7.4) solution (PBS) to remove the free-floating cells and the remaining adherent bacterial cells were fixed by heating at 60 °C for 60 min. Crystal violet (0.1% w/v) dye was loaded at 100 μL onto each well for 15 min at room

temperature then the excessive dye was discarded, and the wells was cleansed with distilled water. Subsequently, 200 μL of ethanol (95%) was added to the well and left for 30 min to destain the cells, then the optical densities of the stained adherent bacterial films were measured at 590 nm. To calculate the percentage of bacterial biofilm inhibition the following equation was used:

$$\text{Biofilm inhibition (\%)} = A_C - A_T/A_C \times 100$$

where A_C represents the OD of the negative controls (without the tested compound), and A_T is the OD of the bacterial films with the F4 encapsulated compound.[42] The negative control plate was prepared as mentioned above and inoculated from well A to well D with the pathogenic bacteria while the wells from E to H was filled with sterile TSB media without inoculation nor crystal violet addition and ciprofloxacin was used as positive control against the tested pathogens.[43]

2.9.8. Time-kill kinetics assay. Time-kill assays were performed following the CLSI M26-A guideline with slight modifications. The inoculum of each strain was adjusted to 0.5 McFarland standard (approximately 1.5×10^8 CFU mL^{-1}) and exposed to the F4-encapsulated compound at concentrations of 0.5, 1, 2, and 4 × MIC. Viable bacterial counts were determined at 0, 2, 4, 6, 8, 12, and 24 h of incubation. Untreated bacterial cultures were included as negative controls. At each time point, samples were serially diluted in sterile saline, and aliquots of 200 μL from the appropriate dilutions yielding countable colonies (30–300 CFU per plate) were spread onto Mueller–Hinton agar (MHA) plates. All plates were incubated at 37 °C prior to colony counting. Experiments were performed in triplicate.

2.10. Statistical analysis

All experiments were performed in triplicate, and data are presented as mean ± SD, with statistical significance set at $p < 0.05$. Encapsulation efficiency (EE%), particle size, PDI, and zeta potential were analyzed using one-way ANOVA with Tukey's *post hoc* test to compare formulations (F1–F4). *In vitro* release data of SHA, DLX, and LIDO were evaluated by two-way ANOVA (time and formulation as factors) with Bonferroni's *post hoc* test, and release kinetics were assessed by linear regression (R^2) for zero-order, first-order, Higuchi, and Korsmeyer–Peppas models. Cytotoxicity (MTT assay) was analyzed by non-linear regression to determine CC_{50} values, with group comparisons performed by one-way ANOVA and Dunnett's *post hoc* test against F4. Antibacterial activity (zone of inhibition) was assessed by one-way ANOVA with Tukey's test for each strain, while MIC and MBC were determined in triplicate, with MBC/MIC ratios used to classify activity. Biofilm inhibition was analyzed by two-way ANOVA (strain and concentration as factors) with *post hoc* comparisons against ciprofloxacin. Time-Kill kinetics assay data (log_{10} CFU mL^{-1}) were evaluated by two-way ANOVA (time and concentration as factors) with *post hoc* tests against untreated controls to determine bactericidal effects (≥3-log_{10} reduction). All analyses were performed using GraphPad Prism v9.0 (San Diego, CA, USA).

3. Results and discussion

3.1. Selection of best formulation

3.1.1. Determination of encapsulation of SHA, LIDO and DLX in beeswax (EE%). In our study, the encapsulation process depends on two critical factors as the drug: carrier ratio and amount of additives (tween 80), as too high a ratio can lead to incomplete encapsulation, while too low may result in under-utilizing the carrier's capacity.[44–46] Whereas, additives significantly impact the solubility, dispersibility, and stability of the drug, thus enhancing or hindering the encapsulation efficiency.[47,48] Formulation 4, composed of 500 mg of beeswax and 300 mg of Tween 80, demonstrated the highest encapsulation efficiencies and the most favorable particle characteristics. Specifically, the encapsulation efficiencies were 89.7 ± 1.2% for SHA, 91.3 ± 1.5% for LIDO, and 87.6 ± 1.8% for DLX. This performance is attributed to the increased amount of Tween 80, which enhances emulsification and stabilization of the formulation, thereby improving drug retention within the nanocarrier matrix,[49,50] as presented in Table 2.

3.1.2. Particle size distribution, PDI, and zeta potential for loaded and unloaded beeswax. The particle size distribution, polydispersity index (PDI), and zeta potential provide critical insights into the colloidal stability and homogeneity of the beeswax-based formulations, both loaded and unloaded (Table 2). The blank (unloaded) beeswax formulation exhibited a mean particle size of 95.12 ± 3.56 nm, a PDI of 0.18 ± 0.026, and a zeta potential of −33.02 ± 1.23 mV, indicating a monodisperse and stable system.

Upon loading with SHA, LIDO, and DLX, the formulations showed an expected increase in particle size due to drug

Table 2 Characterization of nanocarrier formulations: particle size, zeta potential, and encapsulation efficiency of SHA, LIDO and DLX[a]

Formulation	Ratio of drug: nano carrier	Mean particle size (diameter in nm)	Dispersity (PDI)[b]	Zeta potential (mV)	Encapsulation efficiency (EE%)		
					SHA	LIDO	DLX
Blank (beeswax)	—	95.12 ± 3.56	0.18 ± 0.026	−33.02 ± 1.23	—		—
Formulation 1	1 : 3	122.02 ± 2.49	0.44 ± 0.05	−26.16 ± 1.87	68.3 ± 2.1	72.5 ± 1.8	65.2 ± 2.4
Formulation 2	1 : 5	130.16 ± 4.02	0.41 ± 0.026	−28.35 ± 2.69	75.8 ± 1.6	78.2 ± 2.0	71.4 ± 1.9
Formulation 3	1 : 4	127.46 ± 3.89	0.38 ± 0.055	−28.97 ± 1.29	82.1 ± 1.4	84.6 ± 1.7	79.3 ± 2.1
Formulation 4	1 : 5	115.68 ± 2.85	0.26 ± 0.020	−31.70 ± 2.34	89.7 ± 1.2	91.3 ± 1.5	87.6 ± 1.8

[a] Data are expressed as means ± SD (mean ± SD, $n = 3$). [b] Polymodal refers to PDI values that exceed 0.3, while monomodal refers to PDI values below 0.3.

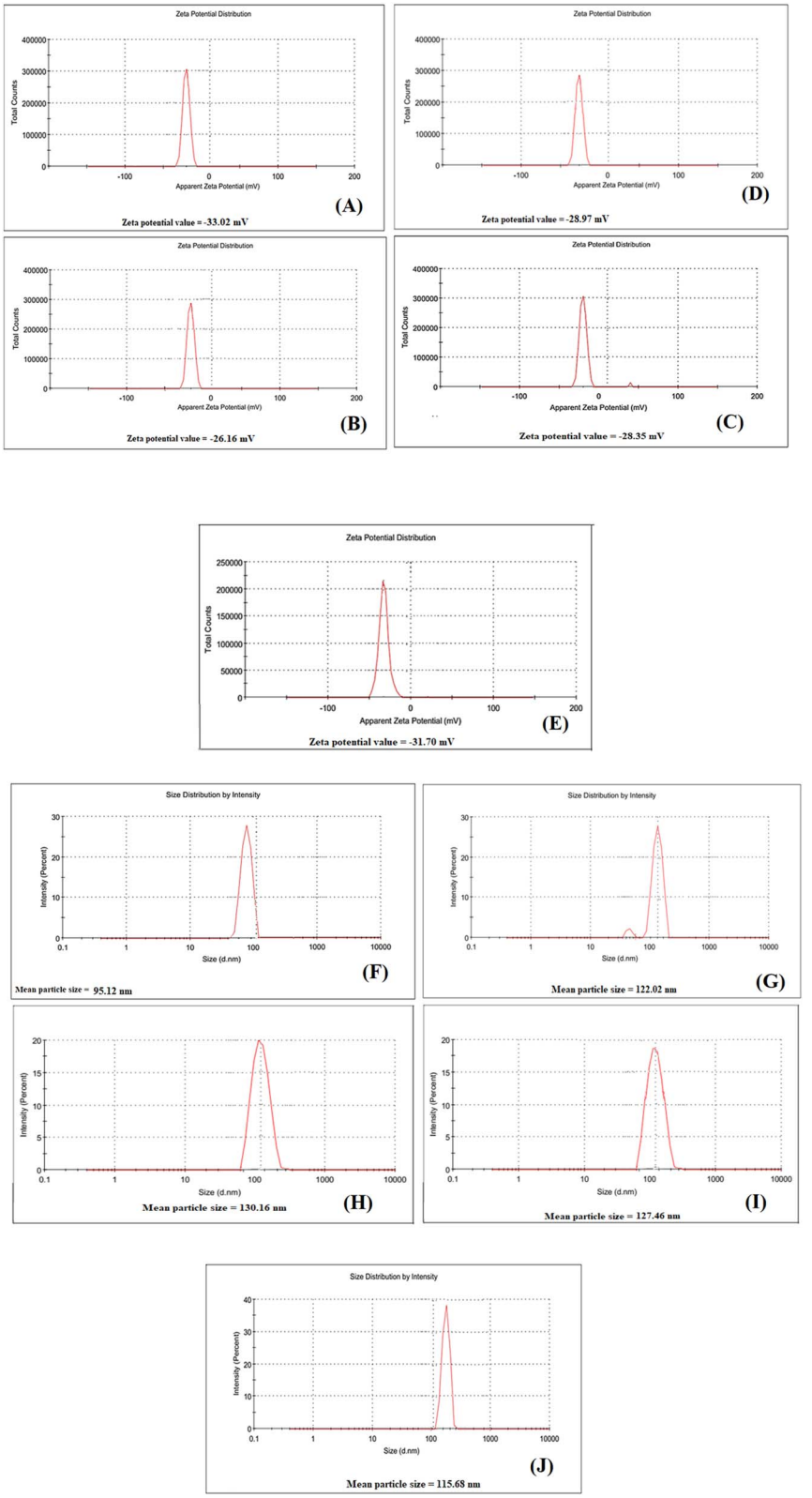

Fig. 2 (A–E) Zeta potential distribution demonstrating an increase in surface charge, increasing colloidal stability and reducing aggregation for the encapsulated formulations compared to the blank formulation. Data are expressed as mean ± SD and were analyzed using one-way ANOVA followed by Tukey's *post hoc* test, with $p < 0.05$ considered statistically significant. (F–J) Dynamic light scattering (DLS) analysis showing the particle size distribution of the encapsulated formulation, indicating a significant reduction in size compared with that of the blank formulation. Data are expressed as mean ± SD and were analyzed using one-way ANOVA followed by Tukey's *post hoc* test, with $p < 0.05$ considered statistically significant.

incorporation. For example, formulation 1 exhibited a particle size of 122.02 ± 2.49 nm and a PDI of 0.44 ± 0.05, suggesting a polymodal distribution (PDI > 0.3). In contrast, formulation 4 achieved a particle size of 115.68 ± 2.85 nm and a PDI of 0.26 ± 0.020, indicative of a more uniform, monodisperse system (PDI < 0.3).

The zeta potential of formulation 4 was −31.70 ± 2.34 mV, showing only a slight reduction from the blank formulation, which reflects adequate surface charge to prevent particle aggregation. So, these attributes including high encapsulation efficiency, low particle size, low PDI, and stable zeta potential have confirmed formulation 4 as the most promising candidate for optimized delivery in wound healing applications (Fig. 2A–J).

3.2. Characterization of encapsulated formulation (F4)

The FTIR analysis was conducted to examine the spectral profiles of lidocaine, delafloxacin, beeswax (Fig. 3), and their composite formulation. A comparative assessment of the obtained spectra is presented in Fig. 4. The FTIR spectrum of pure lidocaine manifested diagnostic absorption bands at 3461 cm^{-1} and 3394 cm^{-1}, corresponding respectively to ν(N–H) vibrations of unassociated amine groups and N–H stretching within the H–N–C=O secondary amide functionality.[51,52] The infrared spectrum displays a characteristic absorption band at approximately 3168 cm^{-1}, corresponding to the asymmetric stretching vibration $\nu_{as}(CH_3)$ of aromatic groups, which the aromatic ring in lidocaine is 2,6-dimethyl-substituted, meaning there are two –CH_3 groups attached to the benzene ring (Fig. 4a).[53] Furthermore, the observed peak near 3002 cm^{-1} provides additional evidence for the existence of aromatic compounds or alternatively indicates the presence of $\nu_{as}(CH_3)$ vibrations. A prominent absorption band at 2920 cm^{-1}, attributable to the asymmetric C–H stretching vibration (ν_{as}) of the $>CH_2$ group in fatty acids. A corresponding peak at 2847 cm^{-1} arises from the symmetric stretching mode (ν_s) of the CH_2 moiety.[54] Additionally, a broad absorption band observed at 2545 cm^{-1} is consistent with the O–H stretching vibrations characteristic of hydrogen-bonded carboxylic acid dimers. The absorption band observed at 1662 cm^{-1} is indicative of the bending vibration δ(C–N–H) coupled with the stretching mode ν(N–C=O) associated with carboxylate functional groups. Concurrently, the peak at 1541 cm^{-1} arises from the combined δ(C=N–H) bending and ν(N–C) stretching vibrations. Further analysis reveals a distinct band at 1473 cm^{-1}, corresponding to $\delta(CH_2)$ scissoring deformations along with contributions from O–H bending modes.[55] Additionally, the absorption at 1384 cm^{-1} can be attributed to $\gamma(CH_2)$ wagging vibrations superimposed with $\delta(CH_3)$ symmetric deformation modes.[56] Additional peaks were observed at 1259, 1159, 1037, 987, 946, 777, and 603 cm^{-1}, which were attributed to various vibrational modes. These included amide III C–C stretching vibrations, aromatic ring deformation coupled with HNC scissoring motions, in-plane bending of –C–H bonds, ring stretching and breathing modes,

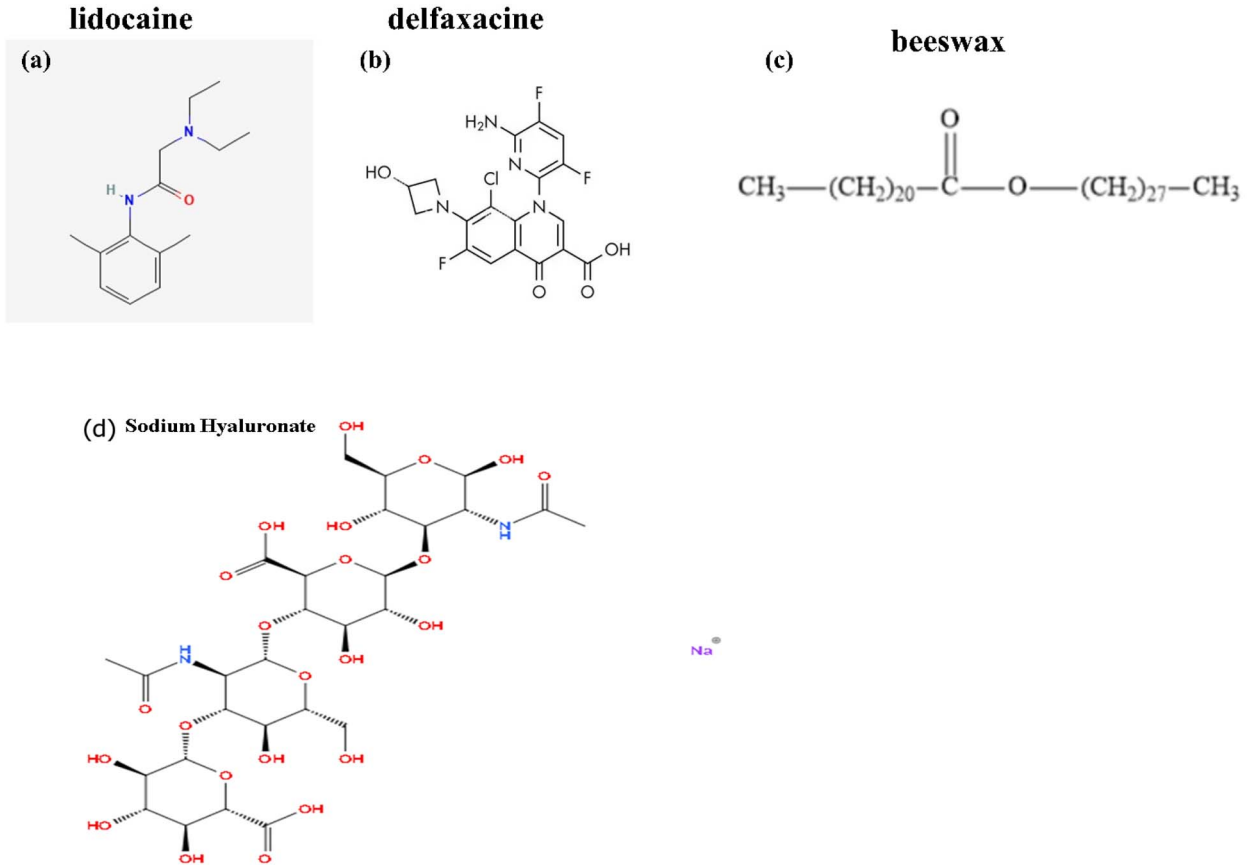

Fig. 3 Chemical structure of (a) lidocaine, (d) delafloxacin, (c) beeswax and (d) sodium hyaluronate.

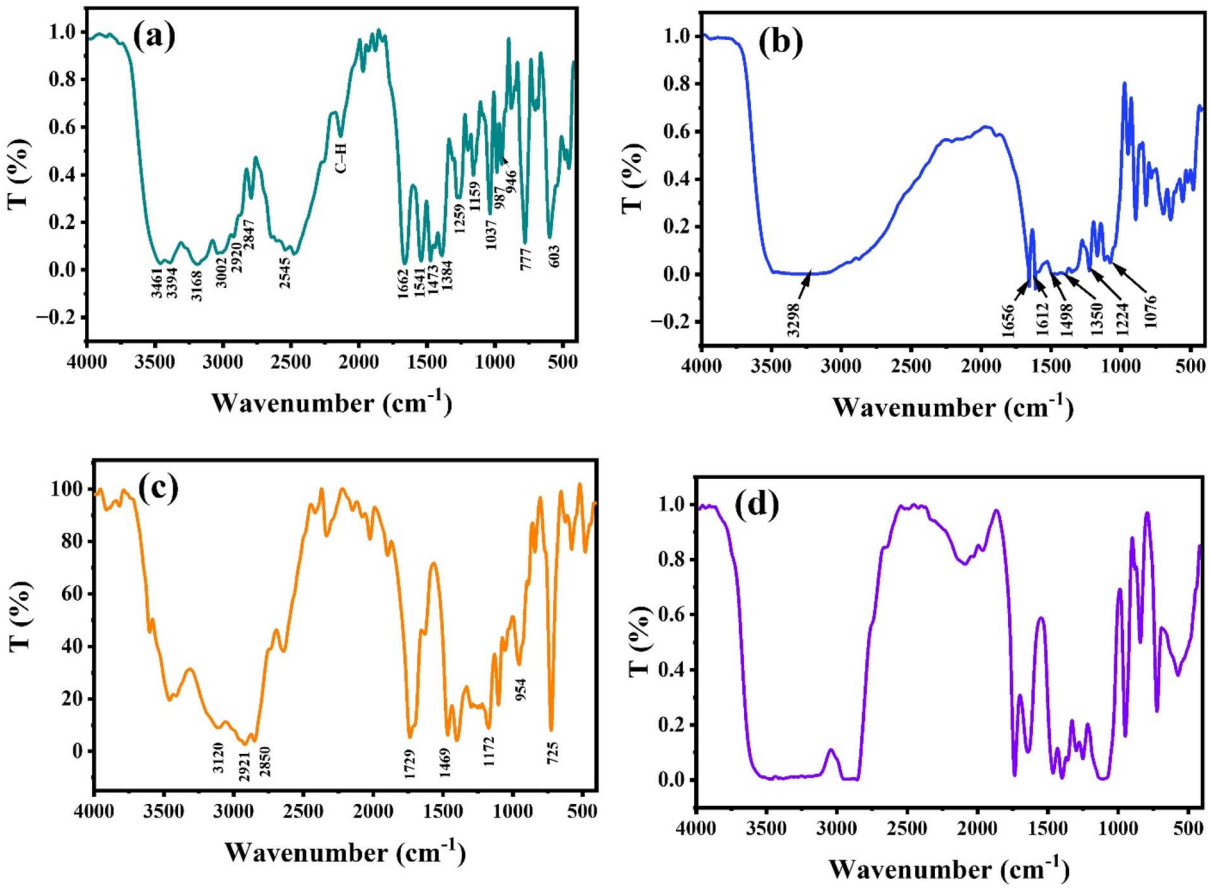

Fig. 4 FTIR spectra of (a) lidocaine, (b) delafloxacin, (c) beeswax, and (d) composite.

as well as $\delta(CH_3)$ C–H rocking vibrations. Additional contributions arose from CH_2 rocking motions combined with aromatic ring –C–H wagging, C–O–C bending and O–H deformations characteristic of dimeric carboxylic acid structures. Further spectral features corresponded to ring torsional modes, out-of-plane CH wagging of aromatic systems, HNC wagging vibrations, and in-plane deformations of C–O bonds.[51,53]

The FTIR spectrum of pure delafloxacin exhibited characteristic vibrational modes corresponding to its functional groups. A prominent broadband centered at 3298 cm^{-1} was assigned to O–H stretching vibrations of hydroxyl groups. The absorption at 1656 cm^{-1} indicated C=O stretching coupled with phenyl ring breathing motions, while the peak at 1612.3 cm^{-1} was attributed to C=C stretching in the α,β-unsaturated ketone moiety (Fig. 4b).[57,58] A distinct band at 1498.5 cm^{-1} confirmed N–O stretching of the nitro functional group, whereas the strong signal at 1454 cm^{-1} arose from C–F stretching vibrations, characteristic of the fluoro substituent. Additionally, C–H bending modes of aliphatic chains were observed at 1350 cm^{-1}.[59] The intense absorption at 1224 cm^{-1} corresponded to C–O stretching overlapping with C–N vibrations, while the peak at 1076 cm^{-1} was indicative of C–O stretching in a primary alcohol (Fig. 4a). These well-defined spectral features strongly support the high purity of the delafloxacin sample.[60,61] For the FTIR analysis of beeswax revealed its characteristic chemical composition, primarily consisting of esterified fatty acids and long-chain alcohols. The material conforms to the general empirical formula $C_{15}H_{31}COOC_{30}H_{61}$, with spectroscopic evidence confirming the presence of key functional groups. Distinct absorption bands corresponding to hydroxyl (–OH) groups, ester carbonyl (C=O) stretches, and alcohol C–O(H) vibrations were identified, consistent with the expected molecular structure of beeswax. These spectral features collectively validate the presence of the fundamental chemical moieties that define the material's composition.[62,63] The FTIR spectrum of purified beeswax, presented in Fig. 4c, reveals several characteristic vibrational modes. A broad absorption band centered at approximately 3120 cm^{-1} corresponds to O–H stretching vibrations, indicative of hydroxyl functional groups. Two distinct peaks observed at 2921 cm^{-1} and 2850 cm^{-1} are assigned to asymmetric and symmetric CH_2 stretching modes, respectively. A discernible absorption feature at 1729 cm^{-1} assigned to the presence of carbonyl (C=O) stretching vibrations.[64] The spectrum further exhibits a CH_2 deformation mode at 1469 cm^{-1}, while absorptions at 1172 cm^{-1} and 725 cm^{-1} are characteristic of ring vibrations associated with the anhydroglucose unit of cellulose. Additionally, a CH_2 rocking vibration is identified at 954 cm^{-1}, completing the spectral fingerprint of the beeswax sample. The absence of spectral bands corresponding to the solvent mixture verified its thorough removal during the drying procedure.[62]

The FTIR spectral analysis of the composite revealed characteristic absorption bands corresponding to the functional groups present in lidocaine, delafloxacin, sodium hyaluronate and beeswax. Notably, an increase in peak intensity was observed for specific vibrational modes, such as a broad hydroxyl (O–H)/(N–H) peak indicates strong hydrogen bonding formation between the loaded molecules and bees wax, typical of polysaccharides, carbonyl (C═O) which confirm the loading of sodium hyaluronate (Fig. 4d), methylene (CH_2), and alkene (C═C) stretching vibrations. Fingerprint region (900–1200 cm^{-1}) contains peaks related to glycosidic linkages and sugar ring vibration related to sodium hyaluronate.

This detailed spectroscopic examination confirms the presence of lidocaine sodium hyaluronate, and delafloxacin within the beeswax matrix, demonstrating their successful incorporation into the composite. These results provide further validation of the effective synthesis of the hybrid material.

3.2.1. Transmission electron microscopy (TEM). The composite was characterized using transmission electron microscopy (TEM). The TEM micrographs presented in Fig. 5 corroborate the homogeneous dispersion of the composite. As depicted in Fig. 5, the nanocrystal (NC) structure displays distinct, quasi-spherical nanoparticles uniformly distributed within the wax matrix. The material is composed of discrete primary nanoparticles, which exhibit a near-spherical morphology and demonstrate excellent dispersibility. These observations align with the documented structural characteristics of beeswax-derived solid nanocarriers.[65] Moreover, the microstructure exhibits a densely populated array of fine, dark particulate features interspersed with discrete, irregular aggregates. This observation suggests a hierarchical organization within the composite, wherein nanoscale spherical entities are uniformly distributed across larger, submicron-sized agglomerates. Such structural characteristics closely resemble those reported for wax-based nanostructured lipid carrier systems. It was observed that the size of the composite nanoparticles was influenced by the addition of the drugs. A slight increase in the average particle diameter occurred when the drug was incorporated. Similar results were reported by different studies.[66]

3.3. *In vitro* release studies

The *in vitro* release profiles of sodium hyaluronate (SHA), delafloxacin (DLX), and lidocaine hydrochloride (LIDO) from the beeswax-encapsulated formulation (F4) demonstrated significant sustained release characteristics across all physiologically relevant pH conditions compared to their free counterparts, aligning with recent advances in biomaterial-based drug delivery systems for wound healing applications,[67,68] as shown in Fig. 6. The encapsulated formulation exhibited markedly controlled release patterns, with SHA showing 82 ± 4.7%, DLX achieving 78 ± 4.4%, and LIDO reaching 85 ± 5.0% cumulative release at 24 hours in acidic conditions (pH 1.2), while free formulations achieved near-complete release (≥99%) within 4–8 hours, demonstrating the efficacy of beeswax as a natural encapsulation matrix for sustained drug delivery, consistent with findings on beeswax solid lipid nanoparticles

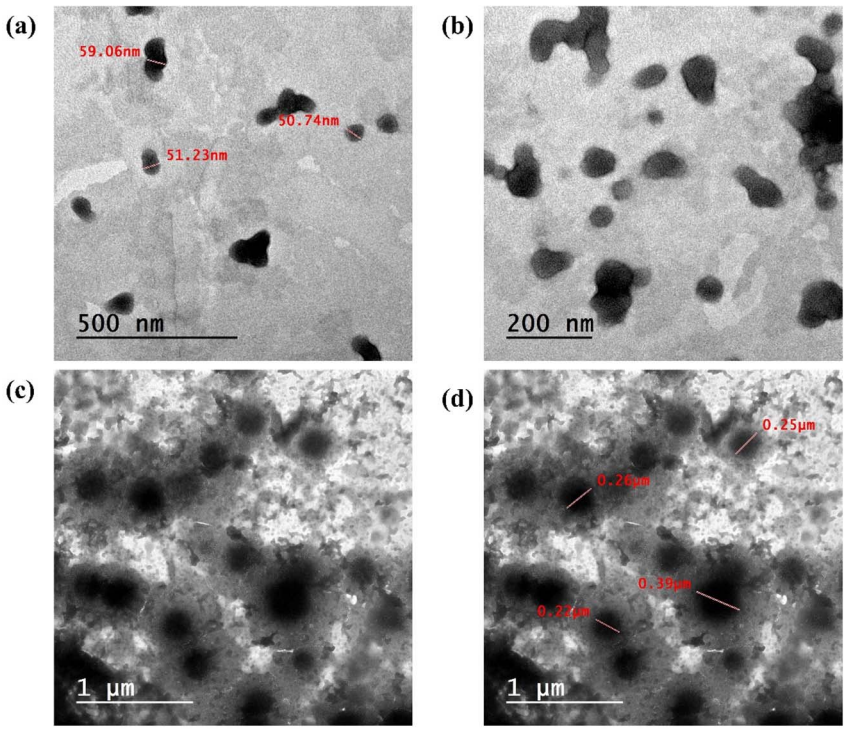

Fig. 5 Transmission electron microscopy (TEM) images of nanostructured lipid carrier composite. (a) Quasi-spherical nanoparticles with diameters of 51.23–59.06 nm uniformly distributed in the wax matrix (scale bar: 500 nm). (b) Higher magnification showing homogeneous dispersion of spherical nanoparticles (scale bar: 200 nm). (c and d) Microstructure revealing hierarchical organization with fine nanoparticles (c) and larger agglomerates ranging from 0.20–0.55 μm (d) (scale bar: 1 μm).

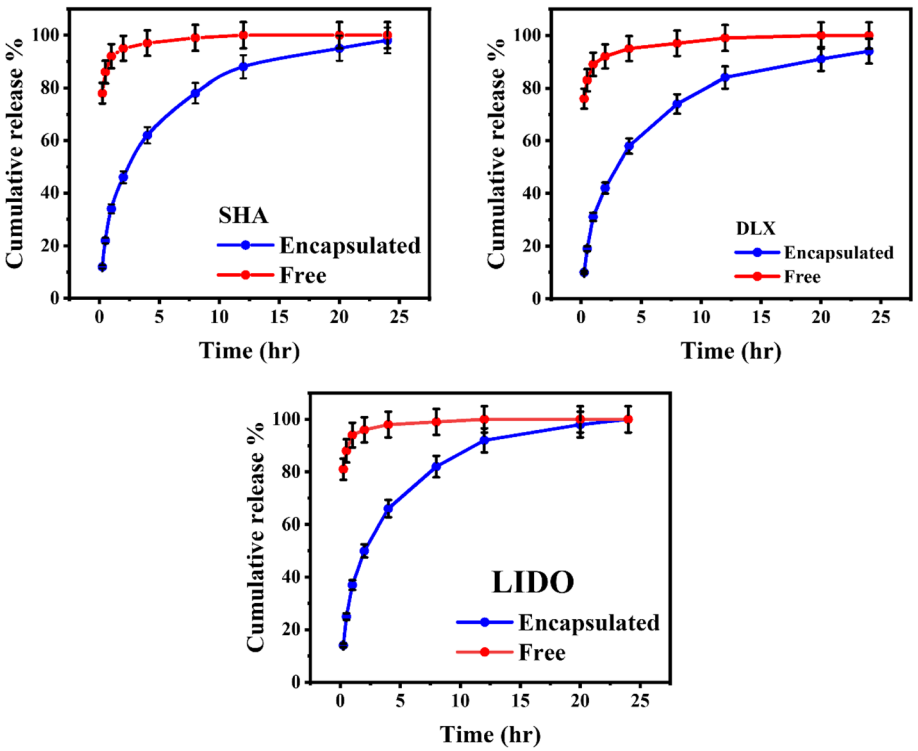

Fig. 6 *In vitro* release profiles of SHA, DLX and LIDO from beeswax composite compared to free forms in PBS (pH 7.4) + SLS over 24 hours. Values represent mean ± SD ($n = 3$).

controlling drug release and improving stability.[67,69] The pH-dependent release behavior revealed enhanced drug liberation at higher pH values, with PBS + SLS medium (pH 7.4) showing the highest release rates (SHA: 98 ± 5.0%, DLX: 94 ± 4.7%, LIDO: 100 ± 5.4% at 24 hours), which is clinically significant as chronic wounds typically exhibit elevated alkaline pH environments (>7.5) compared to healthy skin (pH 4.5–6.5), suggesting optimal drug availability when most needed for therapeutic intervention.[70,71] Notably, delafloxacin demonstrated exceptional performance in acidic conditions, therapeutically advantageous given its enhanced antimicrobial efficacy in acidic environments and the acidic microenvironment of infected chronic wounds due to bacterial metabolism and inflammation, supporting the rationale for this novel fluoroquinolone in wound healing.[72–74] The sustained release profiles observed across all media (HCl pH 1.2, acetate buffer pH 4.5, phosphate buffer pH 6.8, and PBS + SLS pH 7.4) indicate that the beeswax encapsulation system provides controlled drug delivery capable of maintaining therapeutic concentrations over extended periods, potentially reducing dosing frequency and improving patient compliance while ensuring continuous antimicrobial protection, pain management, and tissue regeneration support throughout the complex wound healing process.[67,69] The differential release rates among the three active components (LIDO > SHA > DLX) suggest a tailored release pattern that may provide immediate pain relief through faster lidocaine liberation, followed by sustained hyaluronic acid release for tissue regeneration and prolonged antibiotic coverage through controlled delafloxacin release, representing a sophisticated approach to multi-modal chronic wound therapy addressing the complex pathophysiology of non-healing wounds in diabetic and non-diabetic patients.[67,69,70]

3.4. *In vitro* release kinetics

The *in vitro* release kinetics analysis at physiological PBS pH (7.4) + SLS medium revealed distinct differences in release behavior between encapsulated and free forms of sodium hyaluronate (SHA), delafloxacin (DLX), and lidocaine hydrochloride (LIDO), as shown in Table 3. Across all three compounds, encapsulated formulations exhibited significantly better fitting to first-order ($R^2 > 0.985$) and Korsmeyer–Peppas models ($R^2 > 0.989$), suggesting a diffusion-controlled, concentration-dependent release mechanism, consistent with previous studies on beeswax microspheres demonstrating diffusion-governed drug release profiles,[75] as shown in Fig. 7. In contrast, free formulations demonstrated poor correlation with sustained-release models ($R^2 < 0.89$), confirming an immediate release profile with minimal control over diffusion.

The release exponent (n) values derived from the Korsmeyer–Peppas model for the encapsulated forms were consistently below 0.5 (SHA: 0.43, DLX: 0.48, LIDO: 0.45), indicating Fickian diffusion as the dominant release mechanism. This reflects drug migration through the waxy matrix, where release is governed primarily by passive diffusion rather than polymer erosion or swelling, aligning with findings from flurbiprofen-loaded beeswax microspheres where diffusion was the main release driver.[76] The lower n-values for the free forms ($n < 0.3$)

Table 3 *In vitro* release kinetics data in pH 7.4 (PBS + SLS)

Model	SHA encap. (F4)	SHA free	DLX encap. (F4)	DLX free	LIDO encap. (F4)	LIDO free
Zero-order (R^2)	0.942	0.661	0.968	0.687	0.951	0.703
Zero-order (K_0)	5.42	6.72	5.21	6.68	5.62	6.76
First-order (R^2)	0.988	0.889	0.991	0.873	0.985	0.882
First-order (K)	0.165	5.96	0.152	5.57	0.186	6.58
Higuchi (R^2)	0.974	0.813	0.981	0.797	0.976	0.809
Higuchi (K_H)	22.48	31.54	21.61	31.27	23.47	31.83
Korsmeyer–Peppas (R^2)	0.990	0.886	0.994	0.865	0.989	0.877
Korsmeyer–Peppas (K)	27.26	87.67	25.96	85.74	30.01	89.83
Release exponent (n)	0.43	0.05	0.42	0.06	0.40	0.05

further emphasize their rapid burst release without matrix modulation.

The superior fit to the first-order model, particularly for DLX ($R^2 = 0.991$), reinforces the hypothesis of concentration-gradient-driven release, advantageous in sustaining antimicrobial action over time in wound environments. Similarly, the strong correlation for LIDO ($R^2 = 0.985$) and SHA ($R^2 = 0.988$) in the encapsulated forms supports their sustained availability for analgesic and regenerative functions, respectively. These results echo the controlled release patterns observed in beeswax-based lipid formulations designed for prolonged therapeutic effects.[69]

These findings validate the functional role of beeswax-based encapsulation, which provides a diffusion barrier to modulate the release of hydrophilic and amphipathic agents alike. Notably, the PBS + SLS medium at pH 7.4 mirrors the alkaline microenvironment of chronic wounds, ensuring that the sustained release occurs under clinically relevant conditions.[70] The encapsulation thereby enhances the residence time and local availability of all three therapeutic agents at the site of injury.

The release kinetics confirm that the beeswax matrix effectively prolongs drug liberation *via* Fickian diffusion, while the rapid release from free forms underscores the necessity of encapsulation for sustained therapeutic efficacy in chronic wound management. These controlled release characteristics offer promising translational potential for a single formulation capable of addressing multiple wound healing pathways, including microbial control, inflammation reduction, and tissue regeneration.[69,75,76]

3.5. *In vitro* cytotoxicity evaluation

The MTT assay results demonstrated that the beeswax-based dual-drug nanoformulation (F4) exhibited markedly improved cytocompatibility relative to the unencapsulated free drug combination across all tested concentrations, as shown in Fig. 8. The encapsulated system preserved high cell viability of 98.7 ± 3.2% at 10 μg mL^{-1}, with a gradual, concentration-dependent reduction to 56.8 ± 5.9% at 800 μg mL^{-1}. In contrast, the unencapsulated formulation induced substantially higher cytotoxicity, with cell viability declining sharply to 24.1 ± 6.2% at the same concentration.

This favorable cytotoxicity profile is attributed to the barrier function of beeswax encapsulation, which enables controlled and sustained release of the active compounds while limiting acute cellular exposure, thereby minimizing cytotoxic stress. This mechanism is supported by prior studies indicating that wax-based delivery vehicles can attenuate oxidative and inflammatory cellular responses while maintaining drug efficacy.[77,78] Quantitative analysis of cytotoxic potency (CC_{50}) further supports the protective effect of encapsulation. The CC_{50} values were determined as follows: beeswax (963.21 μg mL^{-1}), F4 formulation (872.40 μg mL^{-1}), SHA (free) (800.55 μg mL^{-1}), LIDO (free) (351.26 μg mL^{-1}), and DLX (free) (210.56 μg mL^{-1}). These results demonstrate that DLX exhibited the highest cytotoxicity, followed by LIDO, whereas SHA and the beeswax matrix were substantially less harmful to cells. The superior safety profile of the F4 formulation, approaching that of beeswax alone, highlights the efficacy of encapsulation in mitigating drug-induced cytotoxic effects.

Importantly, human dermal fibroblasts (HDFs), the cell model used here, are central to wound healing through collagen deposition, extracellular matrix regulation, and tissue remodeling. Preserving their viability is critical for successful wound management, particularly in chronic or diabetic wounds.[79] The observed cytotoxicity pattern supports the general principle that nanoencapsulation enhances the therapeutic index, reducing off-target toxicity while maintaining pharmacological activity.[80,81] Moreover, the encapsulated formulation retained >80% viability up to 200 μg mL^{-1}, surpassing the ISO 10993-5 threshold of 70% viability for cytocompatibility, underscoring its potential clinical safety for topical or local application.[23,82,83] In summary, the MTT cytotoxicity assay underscores the protective and biocompatible nature of beeswax encapsulation, which not only sustains drug availability but also reduces cytotoxic burden, paving the way for clinical translation of this dual-drug delivery platform in wound care, especially among sensitive patient groups requiring minimized toxicity.[84]

3.6. Forced degradation profile and impurity risk assessment

3.6.1. Degradation behavior of APIs and protective role of formulation F4. The forced degradation studies successfully generated degradation within the ICH-recommended range of 5–20%, providing a meaningful impurity profile for toxicological qualification (Fig. S1–S4). The results, summarized in Table S1, reveal the stability of each API and the profound protective effect of the beeswax-based nano-encapsulation in formulation F4.

Delafloxacin (DLX) was the most labile API, with degradation reaching the target range under relevant stresses. Lidocaine

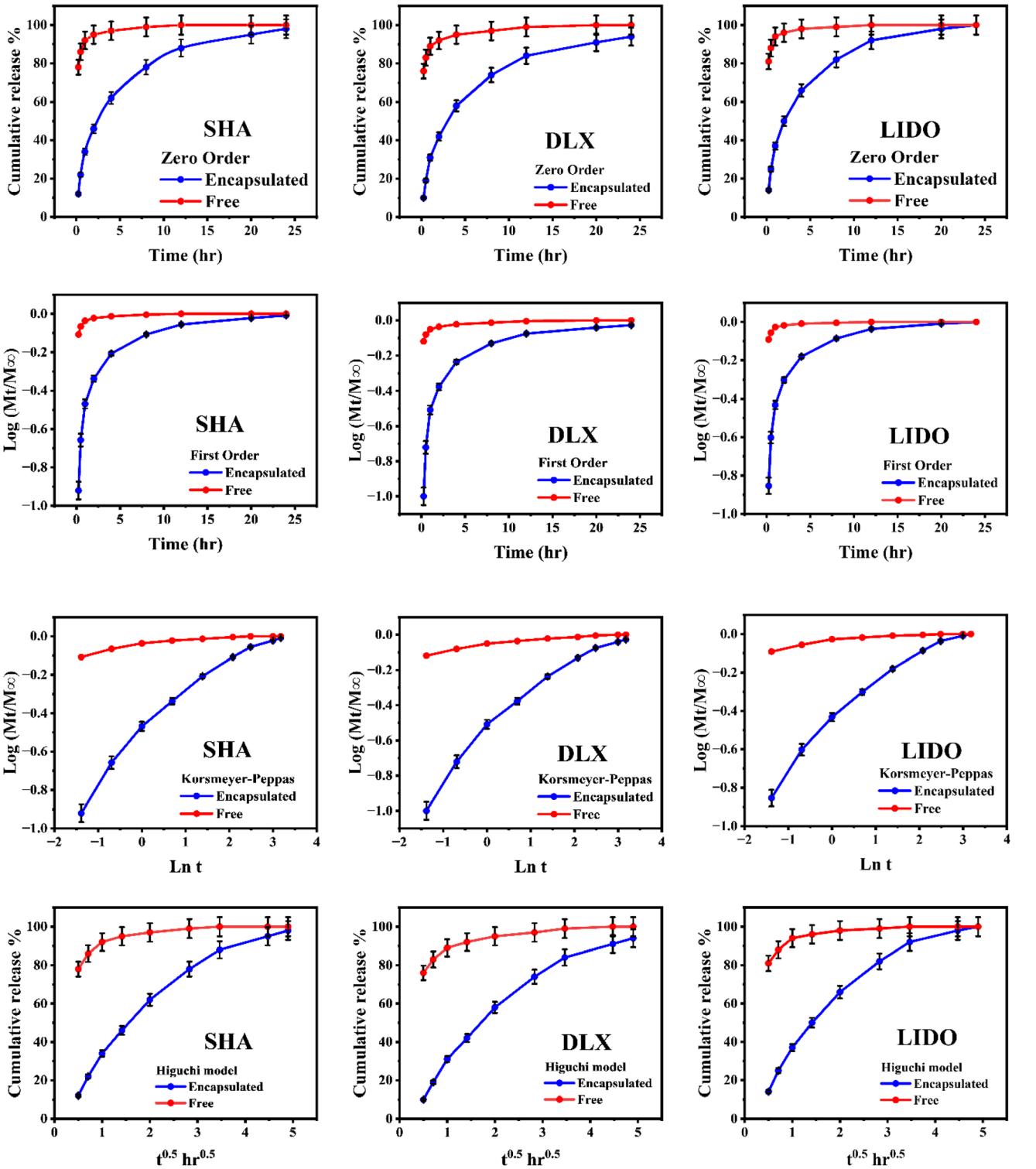

Fig. 7 *In vitro* release profiles of sodium hyaluronate (SHA), delafloxacin (DLX), and lidocaine hydrochloride (LIDO) from free (red) and encapsulated (blue) forms in PBS (pH 7.4, with SLS), fitted to four kinetic models: zero-order (top), first-order (second), Korsmeyer–Peppas (third), and Higuchi (bottom). Values represent mean ± SD ($n = 3$).

(LIDO) showed moderate susceptibility. Crucially, the encapsulated formulation F4 demonstrated a 2 to 3-fold reduction in total API degradation, underscoring the beeswax matrix's role as a protective barrier.

3.6.2. *In silico* impurity and genotoxicity risk assessment per ICH M7. A dual (Q)SAR assessment using complementary methodologies including Toxtree v3.1.0 (expert rule-based: Ames, DNA/protein binding, Cramer Class) and ProTox-3.0

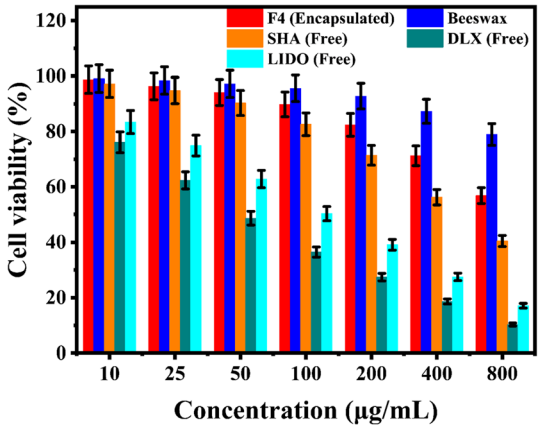

Fig. 8 *In vitro* cytotoxicity evaluation of F4 (encapsulated) and free drug components on Human Dermal Fibroblasts (HDFs) *via* MTT assay. Values are presented as mean ± SD ($n = 3$), with CC_{50} values determined by non-linear regression (dose–response curve fitting). Statistical comparisons were performed using one-way ANOVA followed by Dunnett's *post hoc* test, with $p < 0.05$ considered significant.

(statistical: organ toxicity, LD_{50}) was conducted per ICH M7(R2) Option 4 for all degradants and F4 (Tables 4 and S2). Individual APIs showed mechanism-based alerts (DLX DNA gyrase inhibition: +ve Ames/DNA binding; LIDO low-potency protein binding), but complete F4 formulation yielded negative predictions across all endpoints, classifying impurities as ICH M7 Class 5 (non-mutagenic, no further testing required at ≤1.5 μg per day Threshold of Toxicological Concern (TTC)).[85–87]

To quantitatively assess the DNA interaction potential, molecular docking was performed (Table 5). Delafloxacin demonstrated the strongest binding affinity to the 1TUP DNA duplex ($\Delta G = -8.1$ kcal mol^{-1}), exceeding the control intercalator ethidium bromide ($\Delta G = -7.2$ kcal mol^{-1}). This strong interaction is mechanistically related to its antibiotic activity. Lidocaine and sodium hyaluronate showed weaker binding. When contextualized with the negative Ames test results for the formulation, these docking scores suggest a low risk of clinically relevant genotoxicity from the topical application, as the therapeutic doses are orders of magnitude lower than those required to elicit such effects in mammalian cells. Table S2 documents Class 5 assignments for key degradants (DLX defluorination <0.5%, LIDO *N*-dealkylation <1%, nitrosamine <0.5% in F4), all below reporting thresholds (ICH Q3A/B) with HPLC control.[88,89]

3.6.3. Critical evaluation of nitrosamine risk. A targeted nitrosamine risk assessment was performed in alignment with FDA and EMA guidelines, focusing on the structural alerts

Table 5 Molecular docking results for DNA binding affinity (receptor: 1TUP)

Receptor	Ligand	Binding affinity (ΔG, kcal mol^{-1})
1TUP	Delafloxacin	−8.1
1TUP	Lidocaine	−5.8
1TUP	Sodium hyaluronate	−7.7
1TUP	Ethidium bromide	−7.2

associated with the secondary amine in lidocaine and the tertiary amines in delafloxacin. Under forced nitrosating conditions (0.01% w/v $NaNO_2$, pH 3.0, 37 °C), the free lidocaine API showed the formation of a potential nitrosamine impurity at a level of 2.5%. Crucially, this formation was significantly suppressed in the encapsulated F4 formulation, with the same impurity detected at <0.5%. This result demonstrates that the beeswax encapsulation not only retards standard API degradation but also acts as a chemical barrier against nitrosating agents, substantially mitigating the risk of nitrosamine formation.

3.6.4. Formulation safety and risk contextualization. The ProTox-3 server provided organ-specific toxicity predictions and acute oral toxicity classifications (Table 6). The acute oral toxicity classes are defined as follows: Class III: toxic if swallowed ($50 < LD_{50} \leq 300$ mg kg^{-1}), Class IV: harmful if swallowed ($300 < LD_{50} \leq 2000$ mg kg^{-1}), and Class V: may be harmful if swallowed ($2000 < LD_{50} \leq 5000$ mg kg^{-1}). Delafloxacin was classified as Class V (LD_{50}: 2000–5000 mg kg^{-1}), indicating low acute toxicity, while Lidocaine was Class III (LD_{50}: 50–300 mg kg^{-1}). These predictions must be viewed in the context of the proposed topical application. The therapeutic doses used in wound healing are fractions of a milligram, which are 3 to 5 orders of magnitude lower than these predicted toxic oral doses. Furthermore, dermal absorption for such formulations is typically minimal (<5%), ensuring systemic concentrations remain negligible.

The ASKCOS score of 0.5 confirmed no novel mutagenic interactions. Per ICH M7(R2), Class 5 impurities require no Ames/*in vivo* testing; stability-indicating HPLC ensures control. This suggests a potential for beneficial interactions where the anionic hyaluronate and lipophilic beeswax matrix could modulate the physicochemical environment, potentially stabilizing the drugs and reducing reactive impurity formation, as evidenced by the superior stability of F4 over individual APIs.

In summary, the comprehensive forced degradation and *in silico* assessment confirm that the beeswax-encapsulated formulation F4 offers a dual advantage: it significantly

Table 4 *In silico* toxicity and genotoxicity predictions for formulation components

Compound	Cramer rules	DNA binding	Protein binding	AMES test	Carcinogenicity
Delafloxacin	Class III	+ve (qsna1, qma)	+ve (qsnar)	+ve (qsa28)	+ve (qsa28)
Lidocaine	Class I	+ve (qsna1, qma)	+ve (QMA, Qacyl)	−ve	−ve
Sodium hyaluronate	Class III	−ve	−ve	−ve	−ve
Beeswax	Class I	+ve (QSB)	+ve (QSB)	−ve	−ve
F4 formulation	Class III	−ve	−ve	−ve	−ve

Table 6 ProTox-3 predictions for organ toxicity and acute toxicity classification

Compound	Toxicity class	Predicted organ toxicity (probability >0.5)
Delafloxacin	Class V	Hepatotoxicity (0.60), neurotoxicity (0.73), nephrotoxicity (0.75), respiratory toxicity (0.89)
Sodium hyaluronate	Class IV	Neurotoxicity (0.55), nephrotoxicity (0.84), respiratory toxicity (0.78), cardiotoxicity (0.65)
Lidocaine	Class III	Neurotoxicity (0.90), respiratory toxicity (0.93), BBB permeability (0.90), clinical toxicity (0.78), AChE inhibition (0.55), ecotoxicity (0.64)

reduces the formation of degradation impurities and, based on computational models, presents a low risk of genotoxicity and systemic toxicity, especially when considering the favorable topical administration route and the established clinical safety profiles of its individual components.

3.7. Antibacterial activity

The zone of inhibition method was used for determination of activities of all the ingredients (SHA, Lido, Beeswax, Soya lecithin, Tween 80, F4 encapsulated compound and DLX) included in the formula of the tested F4 encapsulated compound. As observed from Fig. 9 DLX as well as F4 encapsulated compound (512 μg mL^{-1}) showed excellent antibacterial activities against the tested pathogens (*Bacillus subtilis*, *Pseudomonas aeruginosa*, *Escherichia coli* and *Staphylococcus aureus*). Moreover, DLX exhibited lower inhibition zones than the encapsulated compound (F4) against all the tested pathogens, this is a promising result that supports the use of the encapsulated F4 compound as a synergistic compound for the inhibition of bacterial strains under investigation. On the other hand, all the other ingredients showed no activities against the tested pathogens. This result is in agreement with Abu Lila *et al.*[57] who investigated the effect of delafloxacin (DFX) against *Staphylococcus aureus* and *Bacillus subtilis* (as Gram positive pathogens) and *Pseudomonas aeruginosa* as well as *Escherichia coli* (as Gram negative pathogens) and they recorded that DFX was effective against the tested pathogens and the formulated compound (delafloxacin-capped gold nanoparticles) showed higher antimicrobial values than DFX alone.

3.8. Determination of MIC and MBC

To determine the MIC of the tested F4 encapsulated compound as well as the pure delafloxacin antibiotic against the tested bacterial strains (Gram-positive and Gram-negative pathogens), an optical density measurement was used through microdilution flat bottom plates at 630 nm. This was done to determine the efficacy of DLX when loaded in the encapsulated F4 formula. Two-fold serial dilution of DLX or F4 encapsulated compound (at concentration of 512 μg mL^{-1}) fraction was prepared as 128, 32, 8, 2, 0.5, 0.125, 0.031, and 0.0078 μg mL^{-1} to evaluate minimum inhibitory concentration (MIC). Results in Table 7 and Fig. 10 Showed that the MICs of the pure DLX were higher than the formulated F4 compound, since the MICs of DLX against the tested pathogens were 0.125, 0.0078, 0.125 and

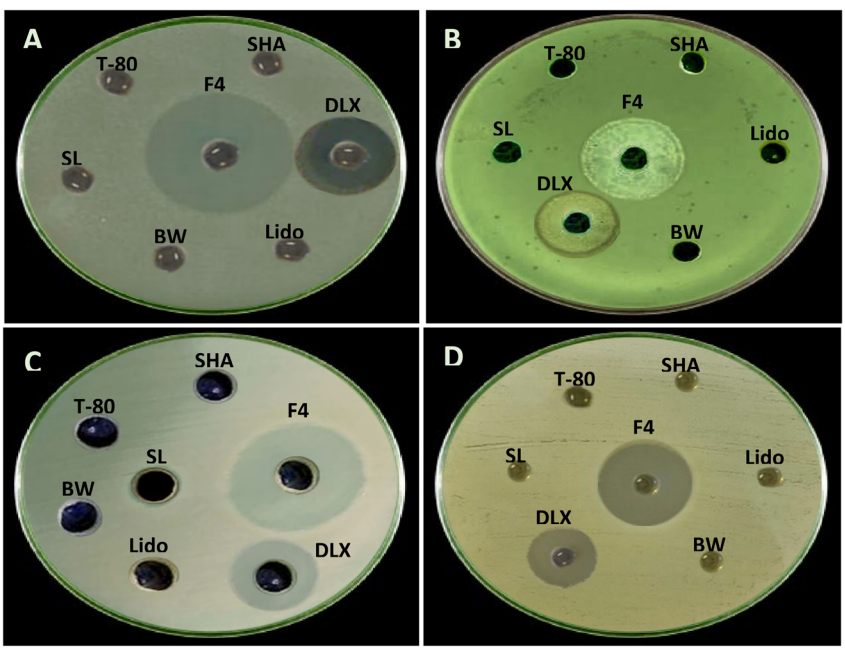

Fig. 9 Zone of inhibition assay of F4, DLX (delafloxacin), SHA (sodium hyaluronate), Lido (lidocaine), BW (beeswax), SL (soya lecithin) and T-80 (Tween 80) against (A) *Bacillus subtilis*, (B) *Pseudomonas aeruginosa*, (C) *Escherichia coli* and (D) *Staphylococcus aureus*.

Table 7 MIC values of delafloxacin and F4 encapsulated compound against selected pathogens[a]

	MIC (μg mL^{-1})	
Strains	Delafloxacin	F4 encapsulated compound
Staphylococcus aureus	0.125	0.031
Bacillus subtilis	0.0078	0.0078
Escherichia coli	0.125	0.031
Pseudomonas aeruginosa	0.0078	0.0078

[a] Experimental notes: (1) All treatments were performed in triplicate. (2) Stock solution concentration: 512 μg mL^{-1} of delafloxacin or the combination, prepared in 70% ethanol. (3) Serial dilution range: 128, 32, 8, 2, 0.5, 0.125, 0.031, and 0.0078 μg mL^{-1}.

0.0078 μg mL^{-1} for *Staphylococcus aureus*, *Bacillus subtilis*, *Escherichia coli* and *Pseudomonas aeruginosa* respectively. On the other hand, the MICs of the encapsulated F4 compound were found to be 0.031, 0.0078, 0.031 and 0.0078 for *S. aureus*, *B. subtilis*, *E. coli* and *P. aeruginosa*. The readings of the results were depending mainly on the concept that the indicator dye (resazurin) serves as redox indicator which was oxidized in the acidic medium caused by bacterial metabolic activities enhancing the color change from blue (no detection of bacterial growth) to pink (resazurin is reduced to resorufin, which has a pink color).

Similarly, Alshememry *et al.*[61] proved that MICs of delafloxacin-loaded poly(D,L-lactide-*co*-glycolide) nanoparticles showed higher sensitivity of *Streptococcus pneumoniae*, *Klebsiella pneumoniae*, *Staphylococcus aureus*, *Bacillus subtilis* and *Escherichia coli* than delafloxacin alone.

Results of MBCs (Table 8) revealed that F4 encapsulated compound showed higher bactericidal rate against *S. aureus* (0.062 μg mL^{-1}), *B. subtilis* (0.0078 μg mL^{-1}), *E. coli* (0.031 μg mL^{-1}) and *P. aeruginosa* (0.0156 μg mL^{-1}) when compared with DLX alone (0.250, 0.0156, 0.250 and 0.0234 μg mL^{-1} for *S. aureus*, *B. subtilis*, *E. coli* and *P. aeruginosa* respectively). Levison stated that the antimicrobial agent is considered as bactericidal material when the MBC/MIC ratio is less than or equal to 4 folds of MIC (MBC/MIC ≤ 4) while when the ratio is less than or equal to 8 folds of MIC the antimicrobial substance is considered as bacteriostatic.[90] From Table 8 it is obvious that MBC/MIC ratios were 2, 2, 2 and 3 in case of DLX against *S. aureus*, *B. subtilis*, *E. coli* and *P. aeruginosa* respectively and 2, 1, 1 and 2 in case of F4

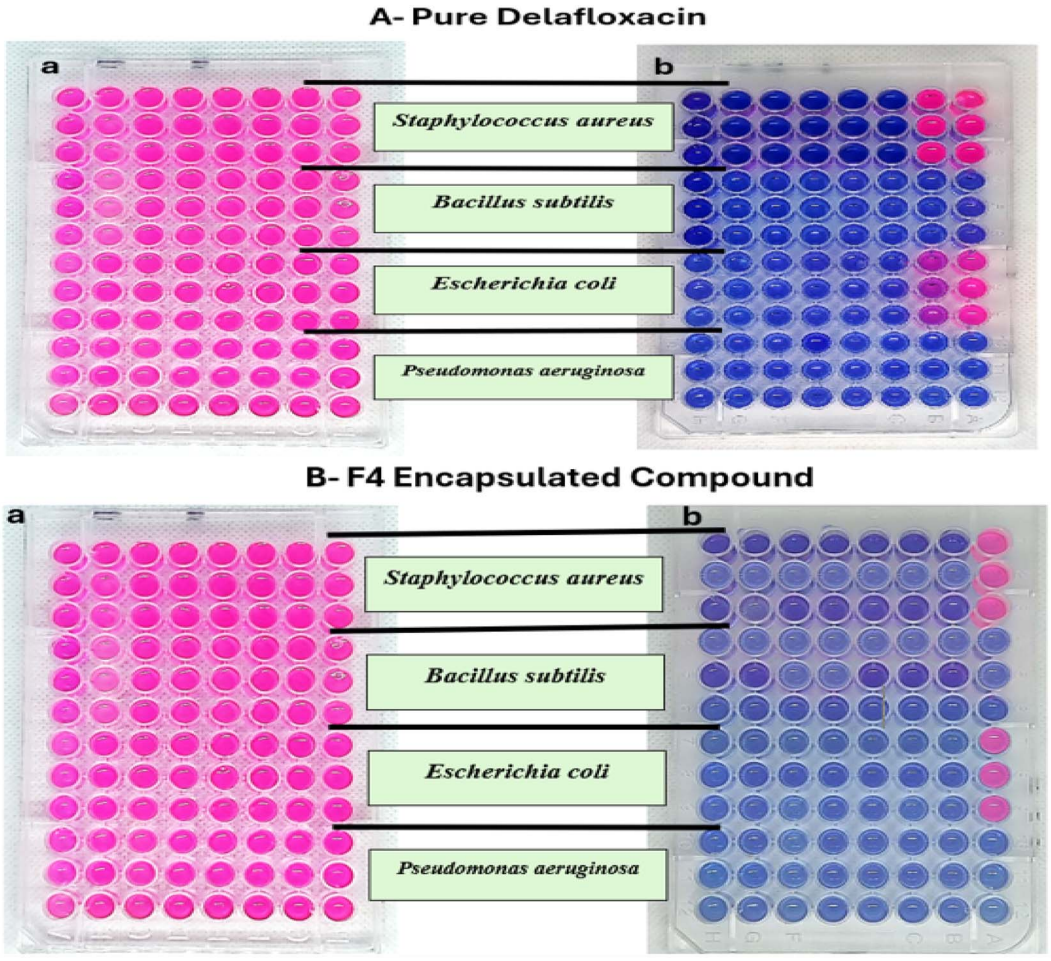

Fig. 10 MICs of DLX (A(b)) and F4 encapsulated compound (B(b)) tested against *Staphylococcus aureus*, *Bacillus subtilis*, *Pseudomonas aeruginosa* and *Escherichia coli*. Bacterial cultures without addition of DLX or F4 encapsulated compound were used as negative control (A(a) and B(a)).

Table 8 MBC values of delafloxacin and F4 encapsulated compound against selected pathogens

	MBC (μg mL^{-1})		MBC/MIC ratio	
Strains	Delafloxacin	F4 encapsulated compound	Delafloxacin	F4 encapsulated compound
Staphylococcus aureus	0.250	0.062	2	2
Bacillus subtilis	0.0156	0.0078	2	1
Escherichia coli	0.250	0.031	2	1
Pseudomonas aeruginosa	0.0234	0.0156	3	2

encapsulated compound against *S. aureus*, *B. subtilis*, *E. coli* and *P. aeruginosa* respectively.

A noticeable difference was observed between the antibacterial response of Gram-positive and Gram-negative bacteria toward the F4 formulation. Gram-positive strains, particularly *Staphylococcus aureus* and *Bacillus subtilis*, showed enhanced susceptibility to the encapsulated formulation, which can be attributed to the simpler structure of their cell wall that facilitates drug penetration. In contrast, Gram-negative bacteria, especially *Pseudomonas aeruginosa*, exhibited a comparatively reduced response, likely due to the presence of an outer membrane and active efflux pump systems that limit intracellular drug accumulation. These structural and physiological differences explain the species-dependent antibacterial performance of the F4 formulation.[91]

The unchanged MIC of delafloxacin (DLX) following its encapsulation within formulation F4 against *Pseudomonas*

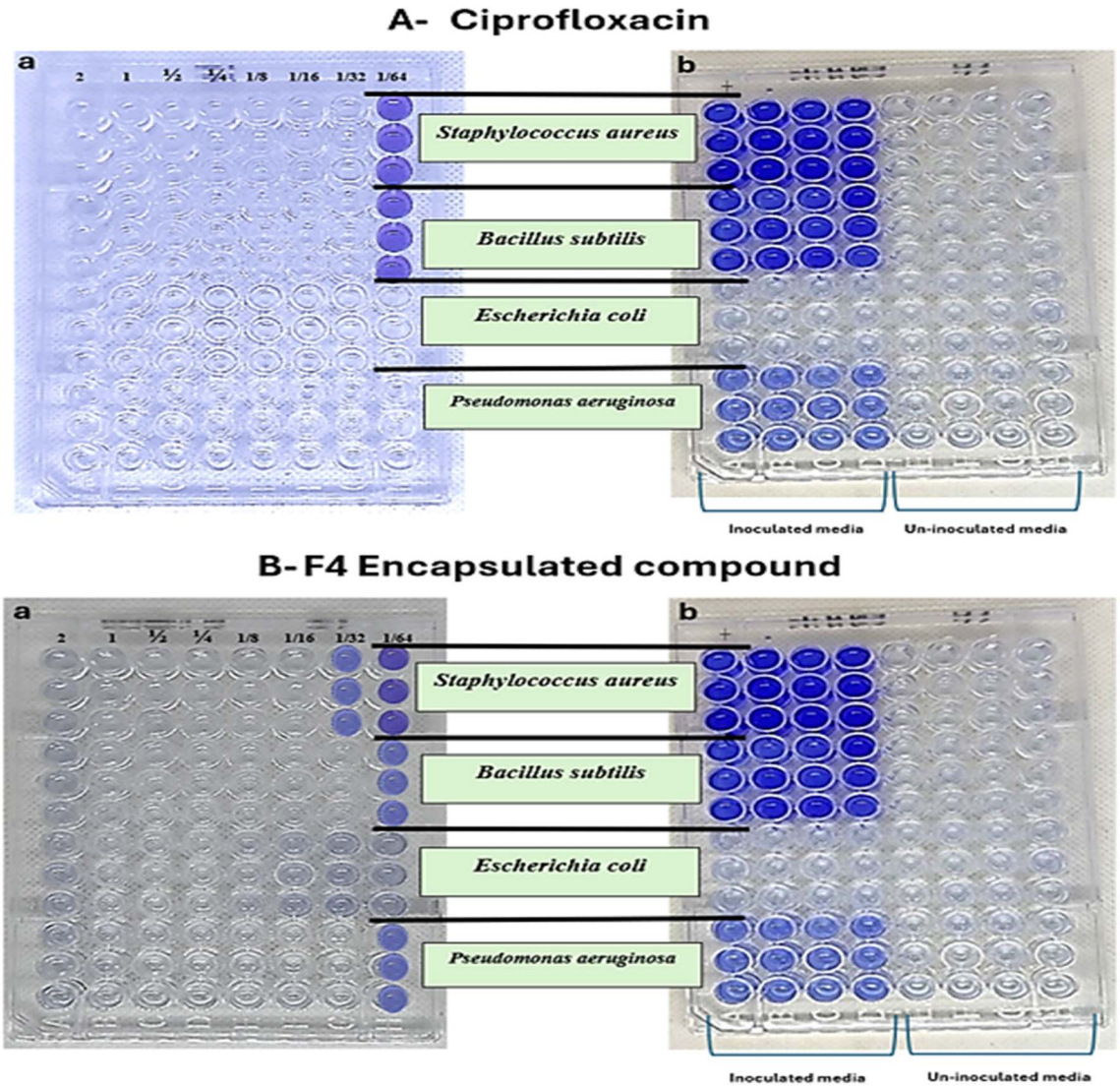

Fig. 11 Antibiofilm of ciprofloxacin (A(a)) and F4 encapsulated compound (B(a)) tested against *Staphylococcus aureus*, *Bacillus subtilis*, *Pseudomonas aeruginosa* and *Escherichia coli*. Bacterial cultures without addition of ciprofloxacin or F4 encapsulated compound were used as negative control (A(b) and B(b)).

Table 9 Time-kill kinetics assay F4 encapsulated compound against *S. aureus* and *P. aeruginosa*[a]

	CFU mL^{-1}									
	S. aureus					*P. aeruginosa*				
Time (h)	Control	0.5 MIC	1 MIC	2 MIC	4 MIC	Control	0.5 MIC	1 MIC	2 MIC	4 MIC
0	1.49×10^8	1.53×10^8	1.44×10^8	1.48×10^8	1.45×10^8	1.63×10^8	1.57×10^8	1.61×10^8	1.55×10^8	1.56×10^8
2	2.14×10^8	1.35×10^8	7.36×10^7	5.89×10^7	4.97×10^7	6.78×10^8	1.33×10^8	1.24×10^8	8.87×10^7	2.82×10^7
4	1.13×10^{10}	7.22×10^7	6.72×10^7	5.11×10^7	4.42×10^7	2.71×10^{10}	1.22×10^8	1.06×10^8	8.25×10^7	3.25×10^7
6	4.6×10^{10}	6.03×10^7	5.52×10^7	3.68×10^7	1.98×10^7	6.78×10^{10}	1.06×10^8	9.3×10^7	7.54×10^7	5.64×10^7
8	1.13×10^{10}	3.77×10^7	2.58×10^7	2.16×10^7	1.29×10^7	1.36×10^{11}	9.22×10^7	7.89×10^7	5.80×10^7	2.98×10^7
12	1.13×10^{10}	2.90×10^7	1.79×10^7	1.75×10^7	1	2.03×10^{11}	7.51×10^7	5.23×10^7	4.29×10^7	9.49×10^6
24	1.13×10^{10}	1.10×10^7	6.44×10^6	4.14×10^6	1	9.49×10^{10}	5.53×10^7	4.72×10^7	2.44×10^7	1

[a] Values below the limit of detection were assigned a value of 1 CFU mL^{-1} for calculation purposes.

aeruginosa is most plausibly explained by the bacterium's pronounced intrinsic resistance mechanisms. *P. aeruginosa* is well recognized for its exceptionally low outer-membrane permeability coupled with the constitutive overexpression of multiple resistance-nodulation-division (RND)-type efflux systems, including MexAB–OprM, MexCD–OprJ, and MexEF–OprN. Collectively, these barriers severely restrict intracellular antibiotic accumulation, ultimately attenuating the therapeutic gains anticipated from advanced encapsulation strategies.[92] The extremely low MIC values observed for free delafloxacin against *Bacillus subtilis* reflect a strong natural sensitivity, which may account for the lack of additional enhancement following encapsulation, likely due to reaching a maximal antibacterial threshold. Furthermore, the variable influence of nano-encapsulation on MIC across different species, especially its restricted effect against multidrug-resistant Gram-negative bacteria such as *Pseudomonas aeruginosa*, is mainly associated with the reduced permeability of the outer membrane and the high activity of efflux transport systems previously documented.[93]

3.9. Antibiofilm assay

Eight concentrations (2-MIC, 1-MIC, $\frac{1}{2}$-MIC, $\frac{1}{4}$MIC, 1/8-MIC, 1/16-MIC, 1/32-MIC and 1/64-MIC) of ciprofloxacin (positive control) as well as F4 encapsulated compound were used to detect the best concentration that cause complete inhibition of biofilm formation by the tested pathogens. Firstly, a control plate was inoculated with the pathogens to determine which of them can/cannot form biofilm (Fig. 11) then it was compared with the positive control antibiotic as well as the tested compound (F4). The results revealed that the encapsulated compound (F4) showed a great antibiofilm activity that was very close to the positive control (ciprofloxacin). The results for F4 compound were 1/16-MIC, 1/32-MIC, 1/64-MIC and 1/32-MIC for *S. aureus*, *B. subtilis*, *E. coli* and *P. aeruginosa* respectively. Moreover, the antibiofilm activity for ciprofloxacin was 1/32-MIC, 1/32-MIC, 1/64-MIC and 1/64-MIC for *S. aureus*, *B. subtilis*, *E. coli* and *P. aeruginosa* respectively.

Biofilms are structured communities of bacteria covered by extracellular polymeric substances (EPSs), such as proteins, polysaccharides and nucleic acids EPSs maintain cell aggregates, provide mechanical stability and protection against antimicrobial agents and are considered a key mechanism for cell adhesion to surfaces of hydrated environments.[94] Ciprofloxacin was used as standard antibiotic due to it is a wide-spectrum antibiotic approved by the FDA against various bacterial infections.[94]

3.10. Time-kill kinetics assay

The procedure was done over a period of 24 h with the pathogenic bacteria (*S. aureus* and *P. aeruginosa*) being exposed to 0.5, 1, 2 and 4-MIC to determine the bactericidal effect of F4 encapsulated compound at several time intervals *i.e.* 0, 2, 4, 6, 8, 12 and 24. Results in Table 9, Fig. 12 showed that bactericidal activity (bacteria completely killed) was observed at higher concentrations (4-MIC) after exposure of 24 h. Interestingly, *S. aureus* demonstrated a shorter time for the bactericidal effect at 4-MIC concentrations within 12 h. The present results are similar to results obtained by Tariq *et al.*[95] who observed that the time killing assay of *Loigolactobacillus coryniformis* BCH-4 metabolites against selected human pathogenic bacteria was performed over a period of 24 h with the pathogenic bacteria, being exposed to 2×, 4×, and 8× MIC of bioactive fraction.

3.11. Study limitations and future perspectives

The current investigation is constrained by several methodological considerations. The exclusive reliance on *in vitro* models (cell cultures and planktonic bacteria) limits direct extrapolation to clinical contexts, as chronic wounds feature complex *in vivo* microenvironments including hypoxia, variable exudate profiles, and established biofilms that may alter formulation performance. Furthermore, antibacterial assessments utilized standard laboratory strains rather than clinically isolated multidrug-resistant pathogens from chronic wounds (*e.g.*, ESKAPE organisms), potentially underestimating real-world antimicrobial challenges. The study also lacked mathematical validation of synergistic interactions between formulation components *via* isobolographic analysis. Additionally, the HPLC-UV methodology employed for nitrosamine risk assessment, while suitable for forced degradation screening, lacks the sensitivity required for definitive identification and quantification of nitrosamine impurities at the stringent regulatory

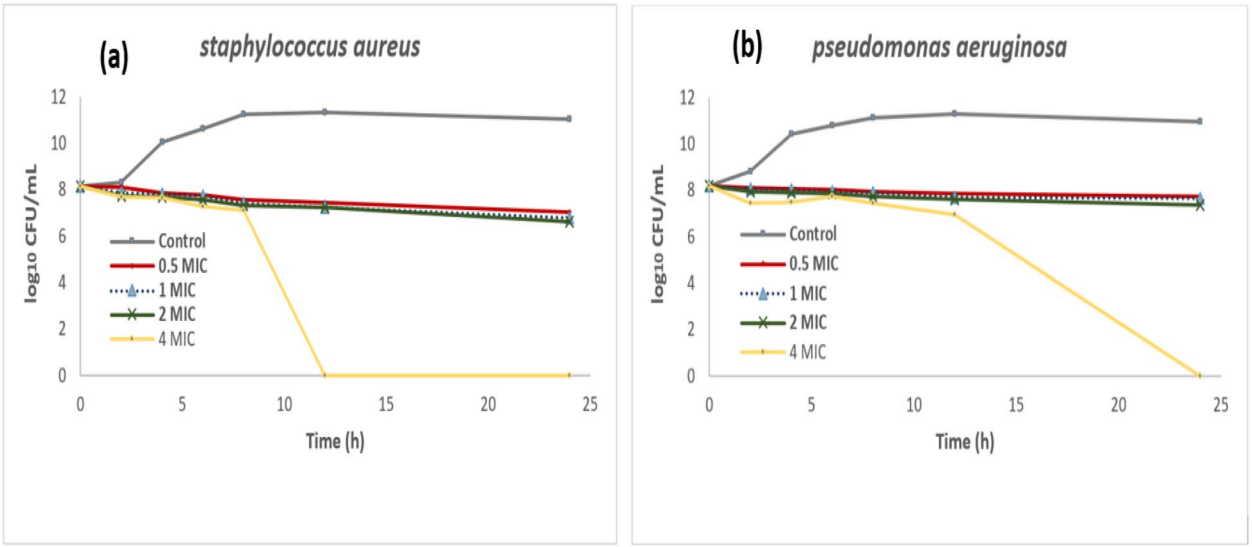

Fig. 12 Time-kill kinetics of the F4-encapsulated compound against (a) *Staphylococcus aureus* and (b) *Pseudomonas aeruginosa*. Viable counts are expressed as $\log_{10}$ CFU mL^{-1} following serial dilution and plating over 24 h.

thresholds, necessitating future confirmatory analysis using LC-MS/MS. Additionally, beeswax's thermolabile nature (melting point: 60–66 °C) presents unquantified storage stability limitations in tropical climates, while the absence of *in vivo* pharmacokinetic data leaves tissue penetration depth and immunogenic responses unverified.

Building upon these findings, subsequent research should prioritize developing polymicrobial biofilm models using clinical isolates embedded in human extracellular matrix analogs to better simulate diabetic wound beds. Rigorous preclinical validation in diabetic murine models with infected full-thickness wounds is essential to quantify bacterial burden reduction, angiogenesis metrics, and local tissue distribution. Concurrently, hybrid encapsulation systems (*e.g.*, beeswax–chitosan composites) warrant exploration to enhance mucoadhesion in exuding wounds while preserving pH-responsive release. The clinical translation pathway should include comprehensive nitrosamine safety verification using LC-MS/MS, phase I safety profiling *via* cutaneous microdialysis in healthy volunteers, followed by dose-finding studies in venous ulcer patients using quantitative wound mapping, culminating in randomized trials against standard-of-care (*e.g.*, collagenase/silver dressings). Expanded applications in burn management and surgical site infection prophylaxis should be investigated, alongside lyophilization protocols for shelf-life extension and GMP-compliant scale-up using high-pressure homogenization.

4. Conclusion

This study successfully engineered an advanced beeswax-encapsulated formulation (F4) integrating delafloxacin, lidocaine, and sodium hyaluronate to holistically address the multifactorial challenges of chronic wounds. The optimized encapsulation strategy achieved exceptional physicochemical stability, uniform drug distribution, and high encapsulation efficiency, while pH-responsive release kinetics governed by a diffusion-controlled mechanism ensure targeted therapeutic delivery aligned with wound microenvironment dynamics. A thorough forced degradation and *in silico* risk assessment confirmed the formulation's stability and low genotoxic potential, underpinning its safety profile. Crucially, the formulation demonstrates synergistic antibacterial potency, significantly lowering MICs against key pathogens, disrupting resilient biofilms at sub-inhibitory concentrations, and exhibiting rapid, concentration-dependent bactericidal action, collectively overcoming key barriers to healing. The significantly enhanced cytocompatibility further underscores its safety for application on compromised tissues. By integrating robust pharmaceutical characterization, microbiological efficacy, and comprehensive safety assessments, this multimodal platform represents a transformative therapeutic paradigm that concurrently targets infection, inflammation, pain, and tissue regeneration. It holds significant potential to accelerate healing, reduce complications, and improve outcomes for high-burden chronic wound populations.

Conflicts of interest

There are no conflicts to declare.

Data availability

The authors confirm that the data supporting the finding of this study are available within the article.

Acknowledgements

This work was supported and funded by the Deanship of Scientific Research at Imam Mohammad Ibn Saud Islamic University (IMSIU) (grant number IMSIU-DDRSP2601).

References

1 C. K. Sen, Human wound and its burden: updated 2022 compendium of estimates, *Adv. Wound Care*, 2023, **12**, 657–670.
2 B. Zhou, A. W. Rayner, E. W. Gregg, K. E. Sheffer, R. M. Carrillo-Larco, J. E. Bennett, J. E. Shaw, C. J. Paciorek, R. K. Singleton and A. B. Pires, Worldwide trends in diabetes prevalence and treatment from 1990 to 2022: a pooled analysis of 1108 population-representative studies with 141 million participants, *Lancet*, 2024, **404**, 2077–2093.
3 L. Guariguata, D. Whiting, C. Weil and N. Unwin, The International Diabetes Federation diabetes atlas methodology for estimating global and national prevalence of diabetes in adults, *Diabetes Res. Clin. Pract.*, 2011, **94**, 322–332.
4 S. Maity, N. Leton, N. Nayak, A. Jha, N. Anand, K. Thompson, D. Boothe, A. Cromer, Y. Garcia and A. Al-Islam, A systematic review of diabetic foot infections: pathogenesis, diagnosis, and management strategies, *Front. Clin. Diabetes Healthc.*, 2024, **5**, 1393309.
5 A. Turban, F. Guérin, A. Dinh and V. Cattoir, Updated review on clinically-relevant properties of delafloxacin, *Antibiotics*, 2023, **12**, 1241.
6 S. C. J. Jorgensen, N. J. Mercuro, S. L. Davis and M. J. Rybak, Delafloxacin: Place in Therapy and Review of Microbiologic, Clinical and Pharmacologic Properties, *Infect. Dis. Ther*, 2018, **7**, 197–217, DOI: 10.1007/s40121-018-0198-x.
7 J. Pullman, J. Gardovskis, B. Farley, E. Sun, M. Quintas, L. Lawrence, R. Ling and S. K. Cammarata, Efficacy and safety of delafloxacin compared with vancomycin plus aztreonam for acute bacterial skin and skin structure infections: A Phase 3, double-blind, randomized study, *J. Antimicrob. Chemother.*, 2017, **72**(12), 3471–3480, DOI: 10.1093/jac/dkx329.
8 L. J. Scott, Delafloxacin: a review in acute bacterial skin and skin structure infections, *Drugs*, 2020, **80**, 1247–1258.
9 A. Adler, S. Chaudhry and T. Goldberg, BaxdelaTM (Delafloxacin): a novel fluoroquinolone for the treatment of acute bacterial skin and skin structure infections, *Pharmacol. Ther.*, 2018, **43**, 662.
10 A. Janowska, G. Papa, M. Romanelli, G. Davini, T. Oranges, C. Stocco, Z. M. Arnez and V. Dini, 5% lidocaine hydrochloride cream for wound pain relief: a multicentre observational study, *J. Investig. Surg.*, 2022, **35**, 49–52.
11 F. Braschi, F. Bartoli, C. Bruni, G. Fiori, C. Fantauzzo, L. Paganelli, A. De Paulis, L. Rasero and M. Matucci-Cerinic, Lidocaine controls pain and allows safe wound bed preparation and debridement of digital ulcers in systemic sclerosis: a retrospective study, *Clin. Rheumatol.*, 2017, **36**, 209–212.
12 H. Hermanns, M. W. Hollmann, M. F. Stevens, P. Lirk, T. Brandenburger, T. Piegeler and R. Werdehausen, Molecular mechanisms of action of systemic lidocaine in acute and chronic pain: a narrative review, *Br. J. Anaesth.*, 2019, **123**, 335–349.
13 J. S. Frenkel, The role of hyaluronan in wound healing, *Int. Wound J.*, 2014, **11**, 159–163.
14 A. Shaharudin and Z. Aziz, Effectiveness of hyaluronic acid and its derivatives on chronic wounds: a systematic review, *J. Wound Care*, 2016, **25**, 585–592.
15 M. Antoszewska, E. M. Sokolewicz and W. Barańska-Rybak, Wide use of hyaluronic acid in the process of wound healing—A rapid review, *Sci. Pharm.*, 2024, **92**, 23.
16 Y. Nong, J. Maloh, N. Natarelli, H. B. Gunt, E. Tristani and R. K. Sivamani, A review of the use of beeswax in skincare, *J. Cosmet. Dermatol.*, 2023, **22**, 2166–2173.
17 K. Gümüş and Z. K. Özlü, The effect of a beeswax, olive oil and Alkanna tinctoria (L.) Tausch mixture on burn injuries: an experimental study with a control group, Complement, *Ther. Med.*, 2017, **34**, 66–73.
18 F. Fratini, G. Cilia, B. Turchi and A. Felicioli, Beeswax: A minireview of its antimicrobial activity and its application in medicine, *Asian Pac. J. Trop. Med.*, 2016, **9**, 839–843.
19 M. Shakeri, S. H. Razavi and S. Shakeri, Carvacrol and astaxanthin co-entrapment in beeswax solid lipid nanoparticles as an efficient nano-system with dual antioxidant and anti-biofilm activities, *LWT*, 2019, **107**, 280–290.
20 P. Fernandez, V. André, J. Rieger and A. Kühnle, Nano-emulsion formation by emulsion phase inversion, *Colloids Surf., A*, 2004, **251**, 53–58.
21 S. M. Mahgoub, M. A. Alwaili, B. R. Alsehli, H. A. Rudayni, A. A. Allam and M. A. Mohamed, Future-proofing RP-HPLC method for quantification of beta-sitosterol in Pygeum extract and cholecalciferol: Promising approaches for prostate health and dietary supplementation, *Acta Chromatogr.*, 2025, **37**(4), 587–595.
22 L. Nobs, F. Buchegger, R. Gurny and E. Allemann, Polymeric nanoporticles as drug delivery systems, *VDI-Ber.*, 2003, 47–62.
23 S. Gruber and A. Nickel, Toxic or not toxic? The specifications of the standard ISO 10993-5 are not explicit enough to yield comparable results in the cytotoxicity assessment of an identical medical device, *Front. Med. Technol.*, 2023, **5**, 1195529.
24 W. Li, J. Zhou and Y. Xu, Study of the in vitro cytotoxicity testing of medical devices, Biomed, *Reports*, 2015, **3**, 617–620.
25 P. Kumar, A. Nagarajan and P. D. Uchil, Analysis of Cell Viability by the MTT Assay, *Cold Spring Harb. Protoc.*, 2018, **6**, 095505.
26 S. R. Mardashev, A. Nikolaev Ya and N. N. Sokolov, Isolation and properties of a homogenous L asparaginase preparation from Pseudomonas fluorescens AG (Russian), *Biokhimiya*, 1975, **40**, 984–989.
27 Z. Tu, S. J. Choure, M. H. Fong, J. Roh, I. Levin, K. Yu, J. F. Joung, N. Morgan, S.-C. Li and X. Sun, ASKCOS: Open-Source, Data-Driven Synthesis Planning, *Acc. Chem. Res.*, 2025, **58**, 1764–1775.

28 G. Patlewicz, N. Jeliazkova, R. J. Safford, A. P. Worth and B. Aleksiev, An evaluation of the implementation of the Cramer classification scheme in the Toxtree software, *SAR QSAR Environ. Res.*, 2008, **19**, 495–524.

29 S. J. Enoch and M. T. D. Cronin, A review of the electrophilic reaction chemistry involved in covalent DNA binding, *Crit. Rev. Toxicol.*, 2010, **40**, 728–748.

30 S. J. Enoch, C. M. Ellison, T. W. Schultz and M. T. D. Cronin, A review of the electrophilic reaction chemistry involved in covalent protein binding relevant to toxicity, *Crit. Rev. Toxicol.*, 2011, **41**, 783–802.

31 R. Benigni, C. Bossa and O. Tcheremenskaia, In vitro cell transformation assays for an integrated, alternative assessment of carcinogenicity: a data-based analysis, *Mutagenesis*, 2013, **28**, 107–116.

32 R. Benigni, C. Bossa and O. Tcheremenskaia, Nongenotoxic carcinogenicity of chemicals: mechanisms of action and early recognition through a new set of structural alerts, *Chem. Rev.*, 2013, **113**, 2940–2957.

33 A. Alhossary, S. D. Handoko, Y. Mu and C.-K. Kwoh, Fast, accurate, and reliable molecular docking with QuickVina 2, *Bioinformatics*, 2015, **31**, 2214–2216.

34 P. Banerjee, E. Kemmler, M. Dunkel and R. Preissner, ProTox 3.0: a webserver for the prediction of toxicity of chemicals, *Nucleic Acids Res.*, 2024, **52**, W513–W520.

35 M. N. Drwal, P. Banerjee, M. Dunkel, M. R. Wettig and R. Preissner, ProTox: a web server for the in silico prediction of rodent oral toxicity, *Nucleic Acids Res.*, 2014, **42**, W53–W58.

36 P. A. Wayne, Clinical and laboratory standards institute: performance standards for antimicrobial susceptibility testing: informational supplement, M100, *Clin. Lab. Stand. Inst.*, 2018.

37 C. H. Teh, W. A. Nazni, A. H. Nurulhusna, A. Norazah and H. L. Lee, Determination of antibacterial activity and minimum inhibitory concentration of larval extract of fly via resazurin-based turbidometric assay, *BMC Microbiol.*, 2017, **17**, 36.

38 R. M. Abdelhameed, M. Abu-Elghait and M. El-Shahat, Engineering titanium-organic framework decorated silver molybdate and silver vanadate as antimicrobial, anticancer agents, and photo-induced hydroxylation reactions, *J. Photochem. Photobiol., A*, 2022, **423**, 113572.

39 M. Abu-Elghait, Determination of Some Virulence Factors in Staphylococcus spp. Isolated from Clinical Samples of Different Egyptian Patients, *World Appl. Sci. J.*, 2014, **32**(4), 731–740.

40 A. M. Shehabeldine, R. M. Ashour, M. M. Okba and F. R. Saber, Callistemon citrinus bioactive metabolites as new inhibitors of methicillin-resistant Staphylococcus aureus biofilm formation, *J. Ethnopharmacol.*, 2020, **254**, 112669.

41 H. Mohd Yusof, N. Abdul Rahman, R. Mohamad, U. Hasanah Zaidan and A. A. Samsudin, Antibacterial potential of biosynthesized zinc oxide nanoparticles against poultry-associated foodborne pathogens: an in vitro study, *Animals*, 2021, **11**, 2093.

42 I. M. Famuyide, A. O. Aro, F. O. Fasina, J. N. Eloff and L. J. McGaw, Antibacterial and antibiofilm activity of acetone leaf extracts of nine under-investigated south African Eugenia and Syzygium (Myrtaceae) species and their selectivity indices, *BMC Complementary Altern. Med.*, 2019, **19**, 141.

43 E. I. Nielsen and L. E. Friberg, Pharmacokinetic-pharmacodynamic modeling of antibacterial drugs, *Pharmacol. Rev.*, 2013, **65**, 1053–1090.

44 H. Hamishehkar, J. Emami, A. R. Najafabadi, K. Gilani, M. Minaiyan, H. Mahdavi and A. Nokhodchi, Influence of carrier particle size, carrier ratio and addition of fine ternary particles on the dry powder inhalation performance of insulin-loaded PLGA microcapsules, *Powder Technol.*, 2010, **201**, 289–295.

45 Z. Peng, S. Li, X. Han, A. O. Al-Youbi, A. S. Bashammakh, M. S. El-Shahawi and R. M. Leblanc, Determination of the composition, encapsulation efficiency and loading capacity in protein drug delivery systems using circular dichroism spectroscopy, *Anal. Chim. Acta*, 2016, **937**, 113–118.

46 M. Novita, N. Suyatma and S. Yuliani, Physical properties of beeswax-oleic acid mixture nanoemulsions as affected by lipid ratio and concentration of emulsifier, *Food Res.*, 2024, **8**, 153–161, DOI: 10.26656/fr.2017.8(6).563.

47 M. Płaczek, D. Wątróbska-Świetlikowska, J. Stefanowicz-Hajduk, M. Drechsler, J. R. Ochocka and M. Sznitowska, Comparison of the in vitro cytotoxicity among phospholipid-based parenteral drug delivery systems: emulsions, liposomes and aqueous lecithin dispersions (WLDs), *Eur. J. Pharm. Sci.*, 2019, **127**, 92–101.

48 V. Pandey and S. Kohli, Lipids and surfactants: the inside story of lipid-based drug delivery systems, *Crit. Rev. Ther. Drug Carrier Syst.*, 2018, **35**(2), 99–155.

49 K. R. Mistry and D. K. Sarker, SLNs can serve as the new brachytherapy seed: determining influence of surfactants on particle size of solid lipid microparticles and development of hydrophobised copper nanoparticles for potential insertion, *J. Chem. Eng. Process Technol.*, 2016, **7**, 302.

50 A. Sukmawati, W. Utami, R. Yuliani, M. Da'i and A. Nafarin, Effect of tween 80 on nanoparticle preparation of modified chitosan for targeted delivery of combination doxorubicin and curcumin analogue, *IOP Conf. Ser. Mater. Sci. Eng.*, 2018, 12024.

51 H. M. Badawi, W. Förner and S. A. Ali, The conformational stability, solvation and the assignments of the experimental infrared, Raman, 1H and 13C NMR spectra of the local anesthetic drug lidocaine, *Spectrochim. Acta, Part A*, 2015, **142**, 382–391.

52 V. L. Chagas, L. dos Santos Silva, C. E. M. de Sousa, R. G. Silva, L. R. de Sousa Carvalho, I. S. S. Silva, J. M. N. Bazán, A. Tofanello, W. Garcia and C. S. Teixeira, Development and characterization of alginate and chitosan hybrid films for dual administration of neomycin and lidocaine, *Int. J. Biol. Macromol.*, 2025, **309**, 142632.

53 P. Agarwal, M. K. Nieuwoudt, S. Li, G. Procter, G. P. Andrews, D. S. Jones and D. Svirskis, Exploiting hydrogen bonding to

enhance lidocaine loading and stability in a poly ethylene-co-vinyl acetate carrier matrix, *Int. J. Pharm.*, 2022, **621**, 121819.

54 S. Bhatia, A. Al-Harrasi, Y. A. Shah, M. Jawad, M. S. Al-Azri, S. Ullah, M. K. Anwer, M. F. Aldawsari, E. Koca and L. Y. Aydemir, Physicochemical characterization and antioxidant properties of chitosan and sodium alginate based films incorporated with ficus extract, *Polymers*, 2023, **15**, 1215.

55 A. Abou-Okeil, M. Rehan, S. M. El-Sawy, M. K. El-Bisi, O. A. Ahmed-Farid and F. A. Abdel-Mohdy, Lidocaine/β-cyclodextrin inclusion complex as drug delivery system, *Eur. Polym. J.*, 2018, **108**, 304–310.

56 H. F. Marei, M. F. Arafa, E. A. Essa and G. M. El Maghraby, Lidocaine as eutectic forming drug for enhanced transdermal delivery of nonsteroidal anti-inflammatory drugs, *J. Drug Delivery Sci. Technol.*, 2021, **61**, 102338.

57 A. S. Abu Lila, B. Huwaimel, A. Alobaida, T. Hussain, Z. Rafi, K. Mehmood, M. H. Abdallah, T. Al Hagbani, S. M. D. Rizvi and A. Moin, Delafloxacin-capped gold nanoparticles (DFX-AuNPs): an effective antibacterial nano-formulation of fluoroquinolone antibiotic, *Materials*, 2022, **15**, 5709.

58 M. K. Anwer, M. Mohammad, N. Y. Khalil, F. Imam, M. J. Ansari, M. F. Aldawsari, F. Shakeel and M. Iqbal, Solubility, thermodynamics and molecular interaction studies of delafloxacin in environmental friendly ionic liquids, *J. Mol. Liq.*, 2020, **305**, 112854.

59 M. K. Anwer, M. Iqbal, M. M. Muharram, M. Mohammad, E. Ezzeldin, M. F. Aldawsari, A. Alalaiwe and F. Imam, Development of lipomer nanoparticles for the enhancement of drug release, anti-microbial activity and bioavailability of delafloxacin, *Pharmaceutics*, 2020, **12**, 252.

60 M. Ramzan, A. M. Yousaf and I. U. Khan, Fabrication and in vitro characterization of delafloxacin-laden electrosprayed hydroxypropyl cellulose nanoparticulated solid dispersions for enhanced aqueous solubility and release rate of the drug, *Int. J. Polym. Mater. Polym. Biomater.*, 2024, **73**, 1367–1373.

61 A. K. Alshememry, M. A. Kalam, M. Shahid, R. Ali, S. S. Alhudaithi, N. A. Alshumaimeri, Z. A. BinHudhud, A. A. Aldaham, Z. Binkhathlan and A. A. Almomen, Delafloxacin-Loaded Poly (d, l-lactide-co-glycolide) Nanoparticles for Topical Ocular Use: In Vitro Characterization and Antimicrobial Activity, *ACS Omega*, 2024, **9**, 50476–50490.

62 L. Svečnjak, S. Prđun, J. Rogina, D. Bubalo and I. Jerković, Characterization of Satsuma mandarin (Citrus unshiu Marc.) nectar-to-honey transformation pathway using FTIR-ATR spectroscopy, *Food Chem.*, 2017, **232**, 286–294.

63 P. Florido-Moreno, J. J. Benítez, J. González-Buesa, J. M. Porras-Vázquez, J. Hierrezuelo, M. Grifé-Ruiz, D. Romero, A. Athanassiou, J. A. Heredia-Guerrero and S. Guzmán-Puyol, Plasticized cellulose bioplastics with beeswax for the fabrication of multifunctional, biodegradable active food packaging, *Food Hydrocolloids*, 2025, **162**, 110933.

64 L. Svečnjak, O. Jović, S. Prđun, J. Rogina, Z. Marijanović, J. Car, M. Matošević and I. Jerković, Influence of beeswax adulteration with paraffin on the composition and quality of honey determined by physico-chemical analyses, 1H NMR, FTIR-ATR and HS-SPME/GC–MS, *Food Chem.*, 2019, **291**, 187–198.

65 K. Liu, H. Liang, J. Nasrallah, L. Chen, L. Huang and Y. Ni, Preparation of the CNC/Ag/beeswax composites for enhancing antibacterial and water resistance properties of paper, *Carbohydr. Polym.*, 2016, **142**, 183–188.

66 I. L. Dantas, K. T. S. Bastos, M. Machado, J. G. Galvao, A. D. Lima, J. K. M. C. Gonsalves, E. D. P. Almeida, A. A. S. Araújo, C. T. de Meneses and V. H. V. Sarmento, Influence of stearic acid and beeswax as solid lipid matrix of lipid nanoparticles containing tacrolimus, *J. Therm. Anal. Calorim.*, 2018, **132**, 1557–1566.

67 M. Shakeri, R. Ghobadi, S. Sohrabvandi, E. Khanniri and N. Mollakhalili-Meybodi, Co-encapsulation of omega-3 and vitamin D3 in beeswax solid lipid nanoparticles to evaluate physicochemical and in vitro release properties, *Front. Nutr.*, 2024, **11**, 1323067.

68 A. P. Cordeiro, P. E. Feuser, P. H. H. Araújo, D. C. Dos Santos, F. Ourique, L. J. Hübner, R. C. Pedrosa and C. Sayer, Doxorubicin and 4-nitrochalcone loaded in beeswax-based nanostructured lipid carriers: In vitro antitumoral screening and evaluation of synergistic effect on HepG-2 cells, *Int. J. Pharm.*, 2024, **666**, 124788.

69 V. Subha, W. Arulsha, S. Kirubanandan and S. Renganathan, Sustained drug delivery of capecitabine using natural (bee wax) and synthetic polymer (PLGA), *MOJ Drug Des. Dev. Ther.*, 2018, **2**, 156–162.

70 R. Brahmi, K. Diaf, Z. Elbahri and M. Baitiche, Preparation and in-vitro evaluation of single and bi-layered beeswax-based microparticles for colon-specific delivery of mesalamine, *J. Serb. Chem. Soc.*, 2024, **89**, 91–106.

71 L. A. Wallace, L. Gwynne and T. Jenkins, Challenges and opportunities of pH in chronic wounds, *Ther. Delivery*, 2019, **10**, 719–735.

72 P. Gupta, K. Vermani and S. Garg, Hydrogels: from controlled release to pH-responsive drug delivery, *Drug Discovery Today*, 2002, **7**, 569–579.

73 M. Rizwan, R. Yahya, A. Hassan, M. Yar, A. D. Azzahari, V. Selvanathan, F. Sonsudin and C. N. Abouloula, pH sensitive hydrogels in drug delivery: Brief history, properties, swelling, and release mechanism, material selection and applications, *Polymers*, 2017, **9**, 137.

74 M. Bhange, K. Vinchurkar, A. Bhadoriya, S. Mane and M. V. Suryawanshi, Recent Advancement in Biomaterial-Based Drug Delivery System, *Des. Process. Green Mater.*, 2025, 293–314.

75 D. V. Gowda, V. K. Gupta, M. S. Khan and A. Bathool, Encapsulation of clozapine into beeswax microspheres: Preparation, characterization and release kinetics, *Int. J. PharmTech Res.*, 2011, **3**, 2199–2207.

76 N. M. Ranjha, H. Khan and S. Naseem, Encapsulation and characterization of controlled release flurbiprofen loaded

microspheres using beeswax as an encapsulating agent, *J. Mater. Sci.:Mater. Med.*, 2010, **21**, 1621–1630.
77 P. Jirwankar, S. Agrawal, F. Shaikh and K. Borse, Natural Excipients: Role in Nano Drug Delivery System, *Curr. Nanomater.*, 2024, **9**, 1–10.
78 V. R. Askari, S. Emarloo, M. S. Fadaei, M. M. Dabbaghi, L. Arabi and V. B. Rahimi, Natural lipids and waxes in drug delivery, *Nat. Biopolym. Drug Deliv.*, 2025, 695–718.
79 H. E. desJardins-Park, D. S. Foster and M. T. Longaker, Fibroblasts and wound healing: an update, *Regener. Med.*, 2018, **13**, 491–495.
80 A. C. Anselmo and S. Mitragotri, An overview of clinical and commercial impact of drug delivery systems, *J. Controlled Release*, 2014, **190**, 15–28.
81 J. Gao, J. M. Karp, R. Langer and N. Joshi, The future of drug delivery, *Chem. Mater.*, 2023, **35**, 359–363.
82 M. A. M. Shafiee, M. A. M. Asri and S. S. S. Alwi, Review on the In Vitro Cytotoxicity Assessment in Accordance to the International Organization for Standardization (ISO), *Malaysian J. Med. Heal. Sci.*, 2021, **17**(2), 261–269.
83 R. Podgórski, M. Wojasiński and T. Ciach, Nanofibrous materials affect the reaction of cytotoxicity assays, *Sci. Rep.*, 2022, **12**, 9047.
84 C. Souza, L. A. P. de Freitas and P. M. B. G. Maia Campos, Topical formulation containing beeswax-based nanoparticles improved in vivo skin barrier function, *AAPS PharmSciTech*, 2017, **18**, 2505–2516.
85 M. R. Q. Ich, M7 Implementation Working Group ICH M7 (R2) Guideline: Assessment and control of DNA reactive (mutagenic) impurities in pharmaceuticals to limit potential carcinogenic risk. Questions and Answers In order to facilitate the implementation of the ICH M7 (R2) Guideline, *The ICH M7 Implementation Working Group has developed a series of Q & As*, 2022, vol. 7.
86 I. H. Guideline, Assessment and control of dna reactive (mutagenic) impurities in pharmaceuticals to limit potential carcinogenic risk M7, in *Int. Conf. Harmon. Tech. Requir. Regist. Pharm. Hum. Use Geneva*, 2014.
87 CH Harmonised Guideline: Assessment and control of DNA reactive (mutagenic) impurities in pharmaceuticals to limit potential carcinogenic risk M7 (R1), *Current Step 4 version*, 2017, https://database.ich.org/sites/default/files/M7_R1_Guideline.pdf.
88 P. E. Smith, Third international conference on harmonization of technical requirements for registration of pharmaceuticals for human use—A toxicologist's perspective, *Toxicol. Pathol.*, 1996, **24**, 519–528.
89 N. Baber, International conference on harmonisation of technical requirements for registration of pharmaceuticals for human use (ICH), *Br. J. Clin. Pharmacol.*, 1994, **37**(5), 401–404.
90 J. H. Sim, N. S. Jamaludin, Y. K. Cheah, S. Halim, N. Binti, A. Halim, H.-L. Seng and E. Tiekink, In vitro antibacterial and time-kill evaluation of phosphanegold(I) dithiocarbamates, R3PAu[S2CN(iPr) CH2CH2OH] for R = Ph, Cy and Et, against a broad range of Gram-positive and Gram-negative bacteria, *Gold Bull.*, 2014, **47**, 225–236, DOI: 10.1007/s13404-014-0144-y.
91 T. J. Silhavy, D. Kahne and S. Walker, The bacterial cell envelope, *Cold Spring Harbor Perspect. Biol.*, 2010, **2**, a000414.
92 A. Elfadadny, R. F. Ragab, M. AlHarbi, F. Badshah, E. Ibáñez-Arancibia, A. Farag, A. O. Hendawy, P. R. De los Ríos-Escalante, M. Aboubakr and S. A. Zakai, Antimicrobial resistance of Pseudomonas aeruginosa: navigating clinical impacts, current resistance trends, and innovations in breaking therapies, *Front. Microbiol.*, 2024, **15**, 1374466.
93 J. M. A. Blair, M. A. Webber, A. J. Baylay, D. O. Ogbolu and L. J. V. Piddock, Molecular mechanisms of antibiotic resistance, *Nat. Rev. Microbiol.*, 2015, **13**, 42–51.
94 R. Stancheva, T. Paunova-Krasteva, T. Topouzova-Hristova, S. Stoitsova, P. Petrov and E. Haladjova, Ciprofloxacin-loaded mixed polymeric micelles as antibiofilm agents, *Pharmaceutics*, 2023, **15**, 1147.
95 A. Tariq, M. Salman, G. Mustafa, A. Tawab, S. Naheed, H. Naz, M. Shahid and H. Ali, Agonistic antibacterial potential of Loigolactobacillus coryniformis BCH-4 metabolites against selected human pathogenic bacteria: An in vitro and in silico approach, *PLoS One*, 2023, **18**, e0289723.